Geothermics 112 (2023) 102743

Contents lists available at ScienceDirect

Geothermics

journal homepage: www.elsevier.com/locate/geothermics

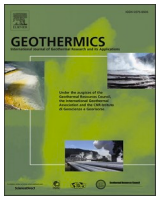

Hydraulic conductivity of the crystalline crust: Insights from hydraulic stimulation and induced seismicity of an enhanced geothermal system pilot reservoir at 6 km depth, Espoo, southern Finland

Ilmo T. Kukkonen [a,b,*], Pekka J. Heikkinen [a,b], Peter E. Malin [c], Joerg Renner [d], Georg Dresen [e], Aino Karjalainen [b], Jussi Rytkönen [b], Juha Solantie [b]

[a] Dept. of Geosciences and Geography, University of Helsinki, P.O. Box 68, Finland
[b] St1, Helsinki, Finland
[c] Advanced Seismic Instrumentation ASIR, United States
[d] Institute for Geology, Mineralogy, and Geophysics, Ruhr-Universität Bochum, Germany
[e] Helmholtz Centre Potsdam, GFZ German Research Centre for Geosciences, Potsdam, Germany

ARTICLE INFO

Keywords:
Geothermal energy
EGS
Hydraulic conductivity
Permeability
Stimulation
Induced seismicity
Crystalline rocks

ABSTRACT

We analyze hydraulic stimulation data from the St1 Deep Heat Project, which comprised drilling wells to >6 km depth in crystalline rock in southern Finland with an aim to study the conditions for an Enhanced Geothermal System. Combining the stimulation and borehole logging data with induced seismicity results allows for a comprehensive analysis of hydraulic conductivity at rarely tested depths of 5 – 6 km. Hydraulic conductivity was observed to be pressure-dependent, heterogeneously distributed and affected by pre-existing fractures and lithological variation. The pre-stimulation formation fracture frequency is in the range of 0 – 8 m^{-1} with an average of 1.9 m^{-1}. Only a small fraction of the fractures were open and conductive implying a hydraulically heterogeneous medium. The average natural hydraulic conductivity derived from leak-off tests and well tests before stimulation and from cross-hole pressure data is of the order of 5 0·10^{-10} - 5 0·10^{-9} m/s (permeability 1·10^{-17} – 1·10^{-16} m^2), which is in agreement with permeability models for the brittle crystalline crust at this depth. Hydraulic stimulation increased conductivity to 10^{-8} – 10^{-7} m/s, but it gradually decreased back to the natural level after pressure release. Stimulation generated five micro-earthquake clusters at 4.8 – 6.3 km TVD depth. Hydraulic connections between clusters were apparently not attained. The project generated extensive experience and data sets regarding deep drilling, hydrogeological properties, and seismic response to stimulation of crystalline rock in the upper continental crust. Hydraulic conductivity turned out to be the most challenging issue for the St1 EGS development and the EGS project is not continued at the moment.

1. Introduction

Hydraulic conductivity is a critically important parameter affecting transport of fluids, heat, and dissolved and particulate matter in groundwater flow, ore-deposit genesis, hydrocarbon exploration and exploitation, nuclear waste disposal, and in utilization of geothermal energy in hot dry rock (HDR) and enhanced geothermal system (EGS) applications as well as in high-enthalpy hydrothermal geothermal systems. Hydraulic conductivity comprises the characteristics of the hydraulic conduits, represented by hydraulic permeability, and properties of the flowing fluid; the conversion factor from permeability to conductivity for water flow in the upper continental crust is $1 \times 10^7 - 3 \times 10^7$ $m^{-1}s^{-1}$ depending on temperature. In crystalline rocks, hydraulic conductivity is typically a rock mass rather than a rock material property. Intact crystalline rock has very small inherent porosity and permeability, but hydraulic connections and flow pathways in rock masses are due to fractures and fracture networks, which vary in frequency, geometry and physical properties (Singhal and Gupta, 1999; Stober and Bucher, 2000a; Schwarz and Zhang, 2003). Fractures likely play an important role for the heterogeneity and scale-dependence of hydraulic properties (Brace, 1984; Clauser 1992; Schulze-Makutch and Malik, 2000; Malin et al., 2020).

Manning and Ingebritsen (1999) and Ingebritsen and Manning (1999) constrained a permeability-depth model for the continental crust

* Corresponding author.
E-mail address: ilmo.kukkonen@helsinki.fi (I.T. Kukkonen).

https://doi.org/10.1016/j.geothermics.2023.102743
Received 13 February 2023; Received in revised form 25 April 2023; Accepted 27 April 2023
Available online 2 May 2023

using geothermal data and fluid fluxes calculated from metamorphic data. In their model, permeability decreases rapidly with depth above the brittle-ductile transition, for example by three orders of magnitude between 1 km and 6 km. Experimental validation of the model is hampered by the scarcity of data (Townend and Zoback, 2000). Drill holes in crystalline rocks are mostly shallower than ~1 km. At such shallow depths, the variation of conductivity values can be considerable such that their tendency to decrease with increasing depth may be overprinted by the general variation of values (McEven and Äikäs, 2000; Mäkelä, 2012). McEwen and Äikäs (2000) reported a variation of five orders of magnitude for injection tests in 30 m long packer-sealed sections at five nuclear waste disposal candidate sites in Finland. The result reflects mostly the effects of fractures at relatively small lithostatic loads. Variation of several decades in conductivity in the uppermost 400 m was reported by Mäkelä (2012) in the central Finland Granitoid Complex from a data set of >1200 water wells. Nuclear waste disposal site studies in Sweden (in crystalline rock, mostly < 1 km depth) have shown similar results, i.e., strong variation of values over several orders of magnitude (10^{-4} – 10^{-12} m/s) in observation scales of 100 – 300 m. Systematic trends with depth are weak or not present. The deepest conductivity values at 1 – 2 km are of the order of 10^{-8} m/s (Walker et al., 1997; Stanfors et al., 1999; Rhén et al., 2009).

Hydraulic conductivity has rarely been measured directly at depths exceeding 1 km due to the lack of boreholes, particularly true for the Fennoscandian Shield. Available measurements are typically related to water wells or surveying bedrock conditions for waste disposal (e.g., Stanfors et al., 1999; Rhén et al., 2009; Pitkänen et al., 1992; Palmen et al., 2004; McEwen and Äikäs, 2000; Posiva 2012; Mäkelä, 2012). The 12 km Kola super-deep hole, NE Russia, revealed the presence of water-bearing open fractures over the complete depth range of the well (Kozlovsky, 1987; Borevsky et al., 1987), and calibrated thermal models suggest hydraulic permeabilities in the range from 10^{-15} m^2 in the upper 2 km to 10^{-21} m^2 at 15 km (Kukkonen and Clauser, 1994; Mottaghy et al., 2005). Hydraulic testing (Ahonen et al., 2011) and fluid logging (Sharma et al., 2015) in the 2.5 km deep research borehole in Outokumpu, eastern Finland (Kukkonen, 2011) showed that hydraulic conductivity decreases rapidly with depth with values in the range of 6.7 $\cdot 10^{-8}$ – 7.5 $0 \cdot 10^{-6}$ m/s. Leak-off-tests (LOT) and drill stem tests (DST) in the 7 km deep drilling in the Siljan impact structure, Sweden, resulted in values in the range of $7 \cdot 10^{-12}$ - 10^{-9} m/s at depths of 1.3 – 6.8 km (Juhlin et al., 1991). Injection tests in deep holes in Germany indicated values of $1 \cdot 10^{-10}$ – $7 \cdot 10^{-9}$ m/s (KTB wells, 0.5 – 9 km; Huenges et al., 1997) and 10^{-10} – 10^{-9} m/s (Urach well, ~4 km; Stober and Bucher, 2000b, Stober 2011). Varying globally from formation to formation, there can be a depth dependence or the data completely lack any trend with depth (Stober and Bucher, 2007; Ranjram et al., 2014). The variability may reflect the effect of present stress field orientation and magnitude on fracture apertures (Banks et al., 1996). Stress is a crucial parameter for hydraulic properties and the most permeable fractures are often the critically stressed ones, i.e., close to shear instability (Ito and Zoback, 2000; Townend and Zoback, 2000). Therefore, the relation between fracture and stress orientation is expected to contribute to the wide range of hydraulic conductivity values recorded even in single wells.

In planning EGS applications in shield areas, the requirement of great drilling depths owing to the low geothermal gradient is thus likely at conflict with the quest for high hydraulic conductivity. A potential remedy for this conflict lies in hydraulic stimulation (Economides and Nolte, 2000; Hofmann et al., 2019; Olasolo et al., 2016; Schill et al., 2017). The company St1 Oy carried out a pilot study of exploring conditions for an Enhanced Geothermal System (EGS) in crystalline bedrock in Espoo, southern Finland, about 5 km NW of downtown Helsinki. The St1 Deep Heat project was in operation 2014 – 2022. The original goal of the project was ambitious: production of 20 – 40 MW of thermal power for a local district heating network (St1, 2018). The project concept was to construct a classical EGS doublet, with injection and production holes of up to 6 – 7 km deep. Thus, the project was the deepest industrial EGS development project in the world so far.

Hydraulic stimulation was applied in the project in 2018 and 2020 to improve hydraulic conductivity. Seismicity induced by stimulation in the St1 project has been analyzed by Kwiatek et al. (2019), Hillers et al. (2020), and Leonhardt et al. (2021). The design and implementation of a traffic light system for stimulation in the St1 project has been described by Ader et al. (2019). Seismic monitoring during and after stimulation as well as structures revealed by seismic while drilling (SWD) and vertical seismic profiling (VSP) have been reported and discussed by Heikkinen et al. (2021).

The present paper focusses on the hydraulic conductivity of the crystalline rocks drilled in the St1 Deep Heat Project and implications of the results for conductivity of crystalline rocks at large and for EGS projects in particular. We discuss the hydraulic conductivity of crystalline crust at the depth of 4.8 – 6.1 km, using hydraulic stimulation data of the St1 project. We analyze data from two deep boreholes with open-hole sections at ~400 m distance from each other and estimate near-wellbore hydraulic conductivity. We demonstrate that the hydraulic conductivity is strongly and non-linearly pressure dependent. Furthermore, we derive and estimate hydraulic conductivity of the rock volume between the holes using cross-hole pressure data recorded in one well during stimulation of the other. To understand the relationships between hydraulic conductivity and structures of the formation, we compare the results with micro-earthquake (MEQ) hypocenter distributions produced by the stimulation, and structures revealed by seismic while drilling (SWD) sounding and vertical seismic profiling (VSP). We show that the stimulations carried out so far did not improve the hydraulic conductivity adequately for using the achieved reservoir as an EGS heat exchanger. We discuss the challenges met with in EGS projects in general and provide an outlook for EGS in crystalline rocks.

2. Drill site geology, hydraulic and geothermal characteristics

The drill site is located in Espoo 5 km NW of downtown Helsinki, Finland (Fig. 1) N60.188395°, E24.827860° The drill site geology is typical for southern Finland (Wennerström et al., 2006; Pajunen, 2008). A thin layer (0–10 m) of Quaternary sediments overlies the Precambrian bedrock. The bedrock comprises c. 1.8 – 1.9 Ga old migmatitic rocks, i.e. mixtures of veined gneiss, mica and hornblende gneisses, amphibolite and granitic intrusions. The lithological boundaries are mostly steep and subvertical. Due to extensive deformation and migmatization during the geological history of the area, the target formation structure is complex. The intact crystalline rock has very low porosity, less than 0.5 vol-%. Therefore, the fluid flow is constrained to brittle deformation structures, i.e., fracture and shear zones. At the surface level, such structures are revealed by several km long linear structures on topographic, geophysical and geological maps. The geothermal gradient is about 17 K/km in the 2 km deep OTN-1 well, and corresponding heat flow is about 52 mWm^{-2}. At 6 km depth, the temperature is about 100 °C.

3. Drilling and drill hole structures

The project comprised drilling three holes (Fig. 1). The collars of all three wells are less than 15 m apart. The pilot hole OTN-1 is 2015 m deep (MD, measured driller's depth) has a diameter of 76 mm, and was completely cored. It was drilled with an inclination of 83 - 69° from horizontal and thus the true vertical depth (TVD) is 1956 m. It was drilled in 2015 to provide baseline information of the rock types, temperature gradient, geophysical properties, and stress field. After drilling, the hole was utilized for seismic observations with a downhole array until 2016 (Heikkinen et al., 2021).

Drilling of the first deep well OTN-2 was started in May 2016. Air hammer drilling was used from 296 m to 3300 m (reached in August 2016). Water hammer drilling was tested, but it did not prove out to be technically reliable, and the final deepening and deviation of the well

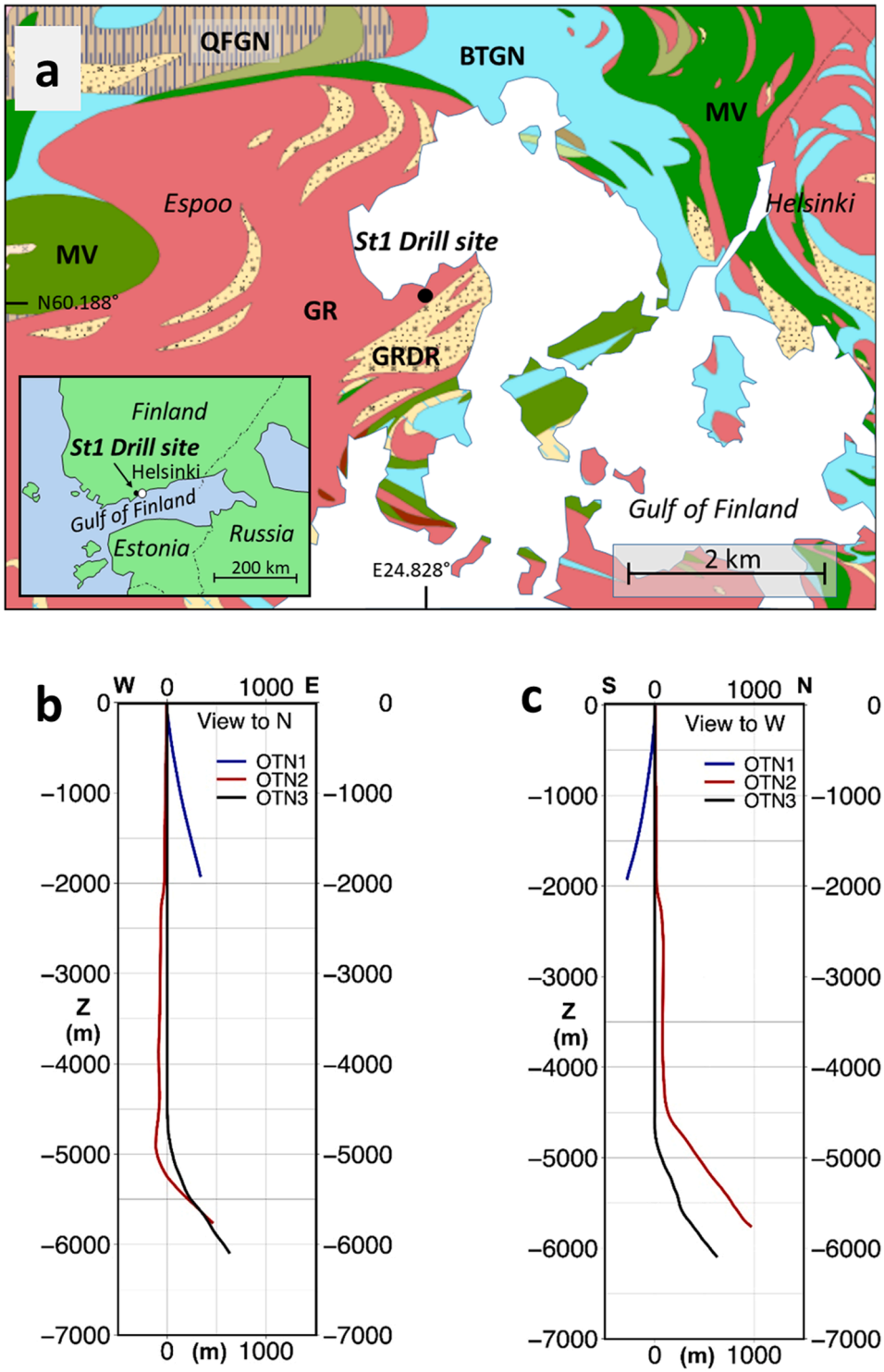

Fig. 1. a) Simplified geological map of the St1 Drill site area (geological data by the Geological Survey of Finland). Rock types: GR, granite; GRDR, granodiorite; BTGN, biotite gneiss, QFGN, quartz feldspar gneiss; MV, mafic volcanic rock, b) W-E projection, and c) S-N projection of the boreholes OTN-1, OTN-2 and OTN-3.

from vertical was done with rotary drilling from January to May 2020.

The drilling of OTN-3 started in August 2016, with air hammering between 300 m and 3300 m, thereafter rotary drilling was applied to 6400 m MD, reached in December 2017. Above 4.0 km both OTN-2 and OTN-3 deviate less than 1° from vertical (Fig. 1). At deeper levels both wells are deviated to NE with final inclinations from vertical of 57° (OTN-2) and 45° (OTN-3). Bit and casing sizes are listed in Table 1 for OTN-2 and OTN-3.

When drilling OTN-3, difficult rock conditions were encountered at about 4.9 km, the top of a major, 400 m thick zone of low seismic velocity. The low velocity is attributed to weak and fractured rock. Repeated attempts to penetrate the zone resulted in three sections of the well: first OTN-3a to 5707 m MD, second OTN-3b, which was successful to 5555 m MD, and finally the third one OTN-3c managed to penetrate the zone and achieved the final MD depth of 6400.10 m.

During deepening of OTN-2 in 2020 the existence of the seismic

Table 1
Bit size and casing data for OTN-2 and OTN-3.

	OTN-2 Depth from	Depth to	OTN-3 Depth from	Depth to
Bit size (inches)				
26	0	296	0	300
17.5	296	2690	300	3000
12.25	2690	4925	3000	5385.7
8.5	4925	6212.5	5356	6400.1
Casing size (inches)				
Surface 18.625	0	296	0	300
Casing 13.375	0	2690	0	2998.5
Liner 9.625	2690	4921	2876	5356
Open hole 8.5	4921	6212.5	5356	6400.1

reflector was known (Heikkinen et al., 2021), and it was decided to direct the deviated part of OTN-2 to run along this zone, interpreted to contain fractures, as it potentially provided higher fracture frequencies and therefore presumably higher inherent hydraulic conductivity. The drilling of OTN-2 resulted in two well versions, OTN-2a (MD 5470 m MD) and OTN-2b (MD 6212.5 m). In the following, the well IDs OTN-2 and OTN-3 refer to the legs OTN-2b and OTN-3c, respectively, unless otherwise noted.

4. Constraints on stress field before stimulations

Understanding stress magnitude and orientation is important for preventing wellbore failure and designing stimulations. It is assumed that stimulation first opens fractures oriented perpendicular to the minimum principal stress. Along with stress field data, fracture orientations and frequency are important for well design. Minimum principal stresses were measured in the OTN-1 pilot hole at eight depth levels between 700 – 1720 m MD using hydraulic mini-fracturing (Becker, 2015; Backers and Meier, 2016). We assumed principal stresses are oriented according to the vertical and horizontal directions. Azimuth of the minimum stress component was determined from wellbore breakouts in OTN-1 (Kukkonen, 2016). The maximum principal stress is horizontal (SH) at azimuth 108°, the intermediate stress is vertical (SV), and the minor horizontal stress (Sh) constitutes the least principal stress indicating the tectonic faulting regime to be dominantly strike-slip, but thrusting occurs in cases (Backers and Meier, 2016). By extrapolating of the stresses and their vertical gradients, determined for 700 to 1720 m depth (Table 2), the tectonic regime is expected to be thrusting at shallower levels and strike-slip at depths >1 – 2 km. Thus, the stress field data suggest that vertical fractures and faults oriented WNW – ESE are optimally oriented for hydrofracturing at target depth of about 5 to 7 km. Consequently, the deviated parts of OTN-2 and OTN-3 were directed to NNE (azimuth 32 - 39°). Assuming hydrostatic fluid pressure, wellhead fluid pressure required to open fractures at target depth was estimated to about ~50 MPa.

Natural EQs in the area before stimulation were shallow (~1 km) thrusting events (M. Uski, Institute of Seismology, University of Helsinki, written communication, 2020), in accord with the stress data extrapolation. Stress polygon analysis (Zoback, 2007) implies that increasing fluid pressure during stimulation (50 - 90 MPa above hydrostatic) favors thrusting over strike-slip events at deeper levels, a prediction in agreement with focal mechanism analysis of stimulation-induced seismic events showing dominantly thrusting (Leonhardt et al., 2021).

Table 2
Gradients of principal stresses at 700 – 1720 m depth for the OTN drill site (Backers and Meier, 2016).

Grad SV	Grad Sh	Grad SH
MPa/km	MPa/km	MPa/km
27.4	16.4	37.7

5. Hydraulic stimulations

Well OTN-3 was stimulated in 2018, and well OTN-2 in 2020. The stimulation of OTN-3 commenced on June 4th, 2018 and lasted 49 days up to July 23rd, 2018. The stimulation was carried out in five stages (depth intervals) starting at the bottom of the open hole section (Table 3) using the Packers Plus® system (Seale et al., 2006). The packer-sealed intervals were 100 – 200 m long (Table 4). The variation in the lengths of the sections was due to considerable wellbore failure. Caliper logging prior to stimulation showed few depth intervals technically suitable for the applied packers (maximum manageable hole diameter <9.5″).

During the OTN-3 stimulation, a total volume of 18,160 m^3 of fresh water was injected over 49 days. Applied constant flow rates were 400 – 800 l/min. The injected fluid was fresh water without chemical additives and proppants. Proppants were not considered useful due to high stresses. Pressure response to injection was measured at the wellhead at 10 – 60 s intervals. The peak pressures recorded at the wellhead were 70 – 90 MPa (Fig. 2).

In OTN-3 stimulation stage 1, five injection tests (leak-off-tests, LOT) were first carried out to estimate the opening pressure of fractures (leak-off pressure, LOP) (Abbott, 2018). Durations of LOTs were 4 – 7 min at average rates of 0.45 m^3/min. The resulting data provided additional information on hydraulic conductivity.

A traffic light (TLS) system required by regulating authorities was applied to control the stimulation procedure in response to observed magnitudes of induced seismic events (Ader et al., 2019). The TLS red light limit was set at magnitude M_L2.1, implying that occurrence of events exceeding this would mean stopping the stimulation. The induced seismicity comprised more than 80,000 micro earthquakes with magnitudes below M_L1.9, most below M_L0.0 (Kwiatek et al., 2019; Leonhardt et al., 2020; Heikkinen et al., 2021). Seismic monitoring was carried out with 12 satellite stations in shallow (300 m) boreholes located within 8 km from the drill site, and a 12 level borehole array in OTN-2 (Kwiatek et al., 2019; Heikkinen et al., 2021). Ground shaking was monitored in eastern Espoo and western Helsinki with up to 17 peak ground velocity (PGV) instruments installed in the terrain and some in the basements of buildings. The highest recorded PGV value was 0.7 m/s. The OTN-3 stimulation produced three earthquake hypocenter clusters located along the open hole section of the well from top to bottom (Fig. 3). Induced seismicity was kept successfully below the limit of magnitude M_L2.1 set by the TLS system by real-time monitoring of seismicity, controlling the injection rates accordingly, and keeping the wellhead pressures <90 MPa (Kwiatek et al., 2019; Heikkinen et al., 2021).

Stimulation of OTN-2 in 2020 was analogous to that of OTN-3 but only one stimulation interval was applied, i.e. the complete open hole section at MD 4.9 – 6.2 km. Before the actual stimulation, hydraulic conductivity tests were carried out with injection durations of 0.5 - 2 h and flow rates of 100 - 600 l/min. In the stimulation of OTN-2, the total volume of fluid (fresh water) injected was much smaller than in OTN-3,

Table 3
Stimulation stages and schedule of stimulation in OTN-3.

Stimulation stage	Start date	Time Finland (UT+3 h)	End date	Time Finland (UT+3 h)
1	6/4/2018	9:27:20	6/15/2018	21:33:46
2	6/16/2018	20:50:56	6/24/2018	0:02:45
3	6/24/2018	8:33:12	7/1/2018	7:46:24
4	7/1/2018	9:55:24	7/12/2018	17:43:24
5	7/12/2018	17:43:24	7/23/2018	19:42:07

Table 4
Depths (MD) of ports and packers in stimulation of the OTN-3 well.

Stimulation stage	Ports	Depth (m)	Packers	Upper packer (m)	Lower packer (m)
1	Port 1	6339.25	Packer 1	6293.42	6400.00
2	Port 2	6247.90	Packer 2	6147.02	6293.42
3	Port 3	6087.02	Packer 3	6042.00	6147.02
4	Port 4	5901.47	Packer 4	5843.89	6042.00
5	D/C frac port	5759.30	Packer 5	5646.75	5843.89

~7000 m^3. Again, fresh water was pumped without chemical additives and proppants. Applied flow rates were 200 – 400 l/min. Pressure response to injection was measured at the wellhead, and the attained peak pressures were 70 MPa, which was also the maximum allowed pumping pressure (Fig. 4). The stimulation was divided into 11 stages (time-wise) and each stage contained up to ten injection (pump) periods lasting about one hour, followed by about 2 h long recovery periods.

Stimulation of OTN-3 well was finished on July 24th, 2018, and the well was shut-in on August 10th. Thereafter the shut-in pressure and pressure decline was recorded at the wellhead during Aug 10 – Oct 13, 2018, until the hole was re-opened for a VSP experiment and temperature logging in October 2018. Data were recorded partly digitally and partly manually. The long-term recordings allowed estimation of the hydraulic conductivity after several months of shut-in time in 2018. After the VSP experiment, the well was shut again and pressure readings were taken semi-regularly. The OTN-3 well was shortly opened for pulling out a seismic borehole array in April 2021. Pressure data were recorded in well OTN-3 during drilling and stimulation of well OTN-2 in February – July 2020, and it provided evidence for a pressure connection between the wells (see Sections 7.2 and Section 7.3). In OTN-2, there has been no pressure monitoring after the end of stimulation.

6. Derivation of hydraulic properties from the stimulation data

The pressure transients recorded during the stimulations of OTN-3 and OTN-2 differ from those reported for hydraulic stimulation of short (< 30 m) intervals (e.g., Zoback et al., 2003; Guljarani and Nolte, 2000). The pressure transients do not show a distinct break-down pressure, indicating fracture initiation, nor is a plateau observed, typically attributed to fracture propagation. Instead, the pressure responses are similar to hydraulic well testing experiments, exhibiting monotonously increasing pressure with pseudo-linear sections at long times and corresponding decay curves recorded during pressure relaxation after end of injection (e.g., Bear, 1979; Fig. 5). We attribute this to the long pressurized depth intervals of 100 m – 1300 m. The fractured rock medium is heterogeneous, and natural fractures favorably oriented for opening and widening exist for every pressure level and new fractures are likely not formed. Nevertheless, the induced seismicity indicates that mechanical slip does occur on fractures due to increased pore pressure. Yet, from the hydraulic viewpoint, the fractured medium responds to fluid injection as a continuum. The absence of pressure fluctuations due to opening of individual fractures may be enhanced by the long distance between the injection interval at 5 – 6 km depth and the pressure gage position at wellhead, which further dampens the response due to the large wellbore storage capacity and viscous losses along the borehole wall. In the present data set, we cannot correlate single seismic events and pressure changes.

In the OTN-3 and OTN-2 data, most of the useful information comes from the late-time parts of the pressure responses. We determined the hydraulic conductivity from plots of pressure (head) vs. log time relying on the Theis model of well drawdown and recovery (see, e.g., Bear, 1979) that assumes a confined, homogeneous and isotropic reservoir. In an injection record, the pressure vs. log time relation becomes linear at times $t \gg r_W^2 S/T$, addressed as late times, for radial flow (Fig. 5), where T denotes transmissivity ($m^2\ s^{-1}$), S storage of the test section (-), and r_W the borehole radius (m). Then, transmissivity of a test section is calculated from the slope of the line (Bear, 1979; Airaksinen, 1978; Domenico and Schwarz, 1998):

$$\Delta s = \frac{2.30Q}{4\pi T}\Delta \log t + \frac{2.30Q}{4\pi T}\log\frac{2.25T}{r_W^2 S} \quad (1)$$

where s is the pressure head (m), t is time (s), and Q is flow rate (m^3/s). Hydraulic conductivity K (m/s) is obtained from

$$K = \frac{T}{b} \quad (2)$$

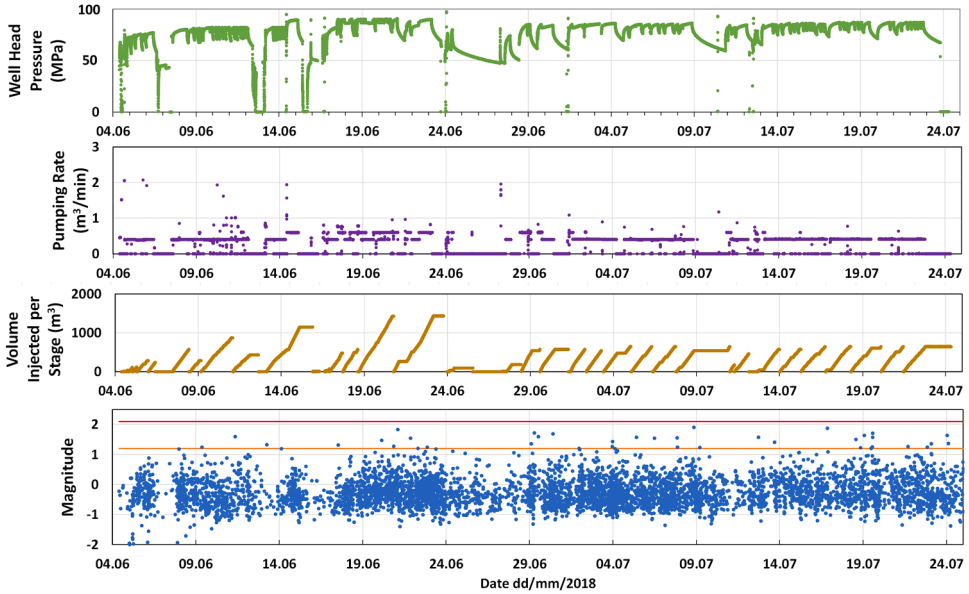

Fig. 2. OTN-3 stimulation data showing stimulation stages, wellhead pressures, injection (pump) rates, cumulative fluid volumes and induced seismicity vs. time. In the lowermost panel, the red and orange lines indicate the magnitude limits of red (M_L2.1) and amber (M_L1.2) events. Data by St1.

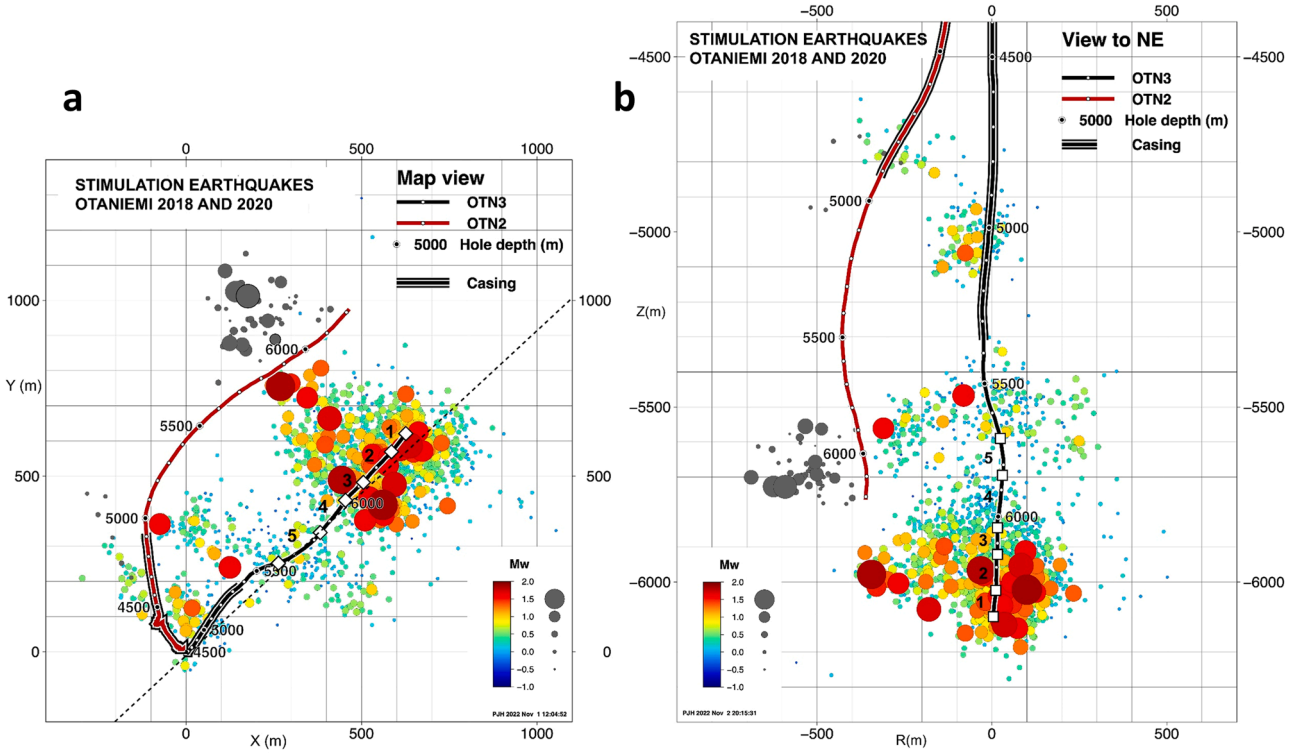

Fig. 3. Micro-earthquake clusters in stimulations 2018 and 2020 (modified from Leonhardt et al., 2021), a) Foci on map view, b) foci on a side view to NE. The colored dots show 2018 events, the gray dots 2020 events. Symbol size is proportional to the estimated rupture area. For 2018 events, colors indicate moment magnitudes. Casing and stimulation stages 1 – 5 are shown. In panel a, the dashed line indicates the location of the cross section in Fig. 9.

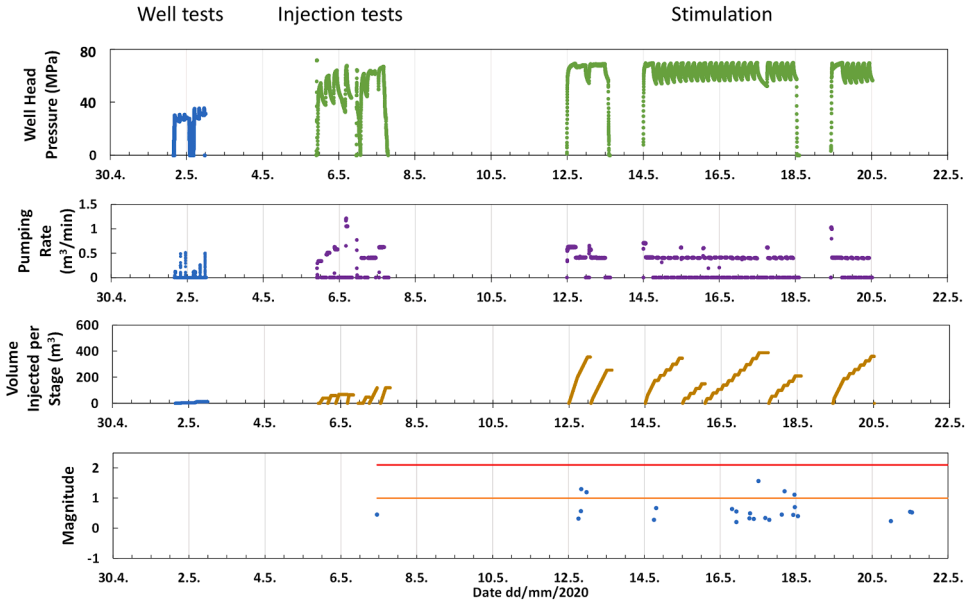

Fig. 4. OTN-2 well tests, injection tests and stimulation data showing wellhead pressures, injection (pump) rates, cumulative fluid volumes and induced seismicity vs. time. Data by St1.

where b is the length of the test section. Hydraulic permeability k (m^2) is obtained from conductivity according to

$$k = \frac{\mu}{\rho g} K \tag{3}$$

where μ is the dynamic viscosity of water (Pa s), ρ the density of water (kg/m^3), and g the acceleration of gravity (9.81 m/s^2). Viscosity of water is temperature dependent, and we applied the approximation for fresh water (Smith and Chapman, 1983)

$$\mu = 2.4{\cdot}10^{-5}{\cdot}10^{\left(\frac{248.37}{\theta+133.15}\right)} \tag{4}$$

where θ is temperature (°C). The reported conductivities represent the temperature 100 °C, which is the approximate formation temperature at

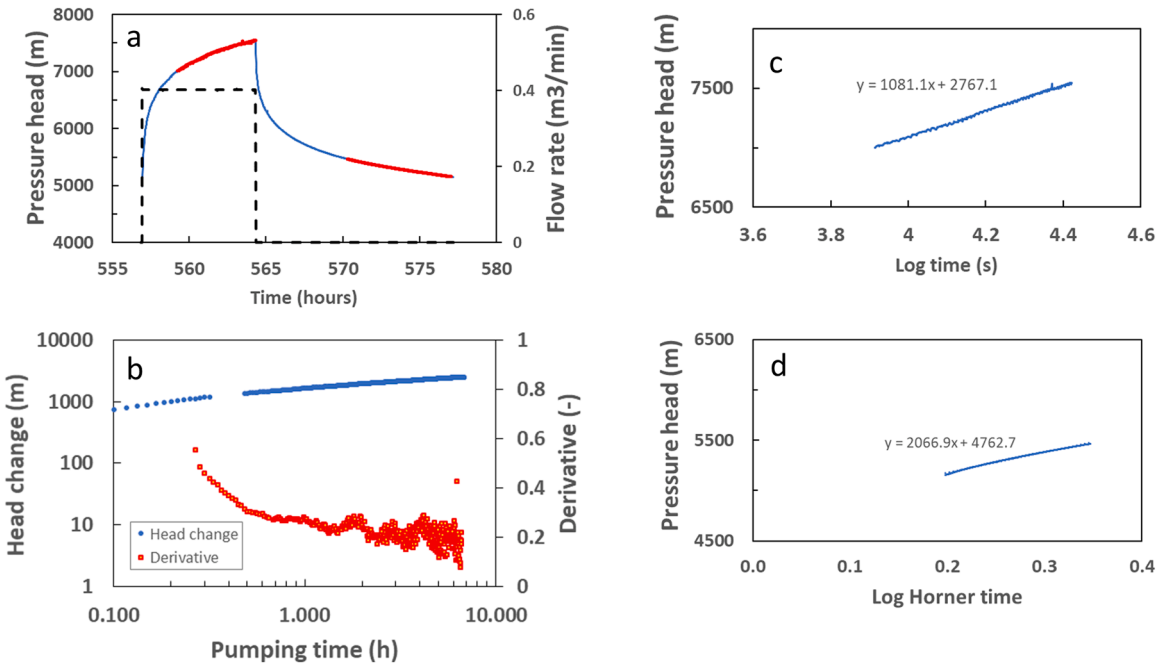

Fig. 5. a) Example of a pressure head (solid line) and flow rate record (dashed line) during injection (7.4 h) and recovery (12.7 h) in OTN-3 stimulation stage 3, pump period 1b. Sections highlighted in red correspond to data in panels c and d; b) plot of head change and log derivative during injection; c) pressure head vs. log time during injection at 2.3 – 7.4 h after start of pumping; d) pressure head vs. non-dimensional time (Horner plot) during recovery at 6.0 – 12.7 h after end of pumping (Horner time 2.25 – 1.57). In panel c and d, the solid lines represent data and the dotted lines regression lines, the slopes of which are used in calculating hydraulic conductivity. Transmissivity correlates with the inverse of the slope (see [1]); the conductivities for injection (c) and recovery (d) are $1.11 \cdot 10^{-8}$ m/s and $5.66 \cdot 10^{-9}$ m/s, respectively.

the depth of the stimulation intervals, i.e., at the vertical depth of 6.1 km. The corresponding permeabilities (m^2) can be obtained by multiplying the conductivity by $2.86 \cdot 10^{-8}$ m s.

The succession of injection and recovery periods necessitates analyzing recovery using the Horner approach (Ehlig-Economides, 1988). Conductivity is estimated from the recovery phase by plotting the pressure head vs. logarithm of non-dimensional time $t_H = (t_{P+} \Delta t) / \Delta t$, where t_P (s) is time used for pumping, and Δt (s) is time after end of pumping. The plot is known as the Horner plot (e.g., Ehlig-Economides, 1988). The slope of the Horner plot at late times provides the transmissivity of the test section using t_H in eq. (1).

Instead of using the approximate solution [1] valid at late times, theoretical modeling with the Theis-well function can also be applied to find transmissivity. Yet, early-time behavior might be affected by deviations of the actual pumping from the step function underlying the theoretical solution. Furthermore, the early-time behavior does not exhibit a diagnostic potential for the flow regime comparable to that of the late-time behavior. It is actually standard practice, to base the identification of the flow regime and the selection of time periods representing linear behavior for conductivity estimation on studying the logarithm of change of the derivative of head vs. log time of the experimental data (log-log plots; Ehlig-Economides, 2000). Radial flow requires a constant log-derivative, a condition that is reached for the performed tests at about 0.5 h (Fig. 5b), indicating a hydraulic diffusivity $D = \frac{T}{S} \sim 10^{-6} - 10^{-5}$ m^2/s.

7. Results

Injection tests in OTN-3 (Stimulation stage 1, MD 6293 – 6400 m) implied that fractures opened at a wellhead pressure of 52 MPa, i.e., the LOP is about 111 MPa at a true vertical depth of 6.1 km (Table 6). For OTN-2, injection tests yielded an opening pressure of 88 MPa corresponding to 34 MPa at wellhead, a result that is not easy to associate with a depth. The long section of the open hole in OTN-2 covered a vertical depth range of 4.83 – 5.77 km. If present, favorably oriented fractures in the uppermost part of the open hole section would open first, and the LOP of 88 MPa then corresponded to a true vertical depth of about 4.8 km. However, the seismic hypocenters from OTN-2 stimulation are located in the lower part of the hole at TVD 5.5 – 5.8 km (Fig. 3), possibly indicating preferential fracture opening there. While the LOP estimates are comparable to the extrapolated smallest stress component (Sh, Table 2) of 92 MPa (corresponding to 38 MPa at wellhead) at 5.6 km and of 100 MPa (corresponding to 46 MPa at wellhead) at 6.1 km, they may indicate a stronger increase in stress gradient with depth at the target depth than that gained from the stress measurements above 2 km.

7.1. Hydraulic properties from stimulation data

Hydraulic conductivities derived from the various test phases range from 10^{-11} m/s to 10^{-7} m/s (Figs. 6& 7, Table 5). Conductivities from OTN-2 stimulation injection and recovery are about one order of magnitude lower than those from corresponding tests in OTN-3 (Fig. 7).

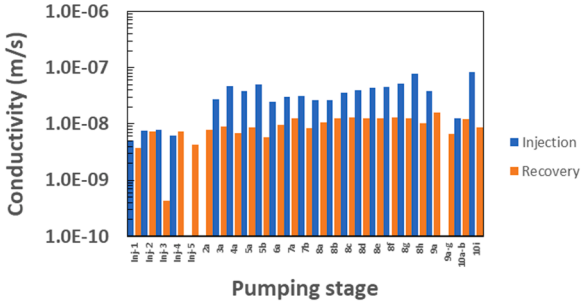

Fig. 6. Conductivities estimated from stimulation of OTN-3, stimulation stage 1, at MD 6293 – 6400 m. Results are shown in chronological order of pumping stages. Blue columns represent data estimated from injection and orange columns data from recovery periods, respectively.

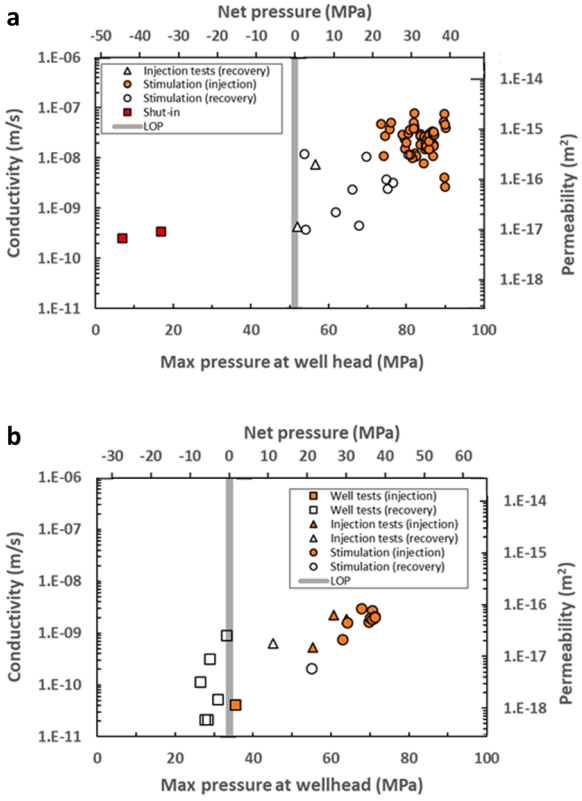

Fig. 7. Hydraulic conductivity (and corresponding permeability) determined from stimulation and shut-in data in OTN-3 (a) and OTN-2 (b). Thick gray lines indicate the LOP (leak-off pressure). Only data determined for late times are included (injection, ≥ 0.5 h; recovery, dimensionless Horner time <1.5).

Despite this quantitative difference, the changes in conductivity over the course of the testing are qualitatively similar for the two wells (Fig. 7). The conductivities estimated from injection are up to an order of magnitude higher than values estimated from recovery data. A distinct development in conductivity values over the course of the stimulations is not obvious, i.e., stimulation did not produce a permanent improvement in conductivity but hydraulic conductivity depends systematically and reversibly on well pressure for both wells (Figs. 6– 7, Tables 5 – 6). Stimulation injection tests correspond to higher mean well pressures than recovery tests, but the two data sets exhibit overlap in covered pressures at least for OTN-3. Conductivity increased with applied injection flow rate and associated pressure increase, but when pressure was relaxed, conductivity returned more or less to its original level (Fig. 6).

The observation of significantly pressure-dependent hydraulic conductivity is not surprising in the light of the pressure range covered by the hydraulic tests in comparison to the estimates for opening pressures (Fig. 6). Above opening pressure, fracture aperture and thus conductivity may significantly increase with an increase in net pressure. The observed pressure dependence might be the cause for the systematic difference between conductivity estimates from injection and recovery, observed even for the pressure range covered by both types of tests (Fig. 6a). Using the conventional late-time solution [1] for media exhibiting a transmissivity increasing with pressure tends to overestimate transmissivity (Wu and Pruess, 2000). For example, during injection the pressure increases less for the pressure-dependent material behavior than for one with a constant transmissivity (e.g., Ortiz et al., 2011), and thus the late-time slopes are lower. The variation in pressure during the linear part of the pressure transient is about twice as high for injection tests as for recovery (Fig. 6), and therefore recovery behavior is less affected by pressure-dependent transmissivity than injection behavior whose analysis leads to relatively overestimated conductivity values. One may well question the validity of applying [1] in an analysis of a medium that exhibits pressure-dependent hydraulic properties. Yet, we take the general consistency of constraints from injection and recovery in magnitude and in their variation with pressure as a-posteriori support. Specialized analyses taking account of the full hydro-mechanical coupling (e.g., Schmidt et al., 2021) will have to be performed, but are beyond the realm of the holistic overview investigation intended here.

7.2. Hydraulic connection between wells

A cross-hole pressure signal was recorded in OTN-3 during stimulation of OTN-2 in 2020 that allows estimation of the average hydraulic properties between the two wells (Fig. 8). The pressure in OTN-3 began to rise about five days after the stimulation was started in OTN-2, and the pressure reached its maximum in five weeks (Fig. 8a). Average hydraulic properties of the rock between the wells were estimated with the Theis model (Bear, 1979) approximating the injection of water in OTN-2 with an 18 days long injection with constant flow rate of 85 l/min using an inter-well distance of 400 m (Fig. 8b). The result represents the average properties along the fastest route for pressure diffusion between the two wells. The estimated hydraulic conductivity of $5{\cdot}10^{-10}$ m/s is of the same order of magnitude as the natural conductivities estimated from leak-off tests and shut-in pressure data in OTN-3 (Fig. 7a, Tables 5 and 6). The lowest conductivities obtained from the well tests in OTN-2 are about an order of magnitude lower ($\sim 5{\cdot}10^{-11}$ m/s, Fig. 7b).

Table 5
Average hydraulic conductivities gained from injection tests, well tests and stimulation stages in OTN-3 and OTN-2.

Operation		Injection				Recovery			
	Depth MD (m)	Average conductivity[1] (m/s)	N	Average conductivity[2] (m/s)	N	Average conductivity[1] (m/s)	N	Average conductivity[3] (m/s)	N
OTN-3									
Injection tests	6293 - 6400	6.63E-09	4	n.a.		3.26E-09	5	1.78E-09	2
Stimulation 1	6293 - 6400	3.73E-08	18	3.96E-08	15	2.61E-08	20	1.06E-08	1
Stimulation 2	6147 - 6293	2.35E-08	11	1.96E-08	9	8.19E-09	7	n.a.	
Stimulation 3	6042 - 6147	1.79E-08	5	1.76E-08	4	3.94E-09	5	2.13E-09	2
Stimulation 4	5844 - 6042	1.68E-08	13	1.84E-08	11	6.32E-09	11	8.32E-10	1
Stimulation 5	5647 - 5844	2.33E-08	33	2.32E-08	31	7.54E-09	33	2.70E-09	6
OTN-2									
Well tests	4921 - 6213	3.25E-10	6	4.13E-11	1	1.87E-10	6	9.62E-11	6
Injection tests	4921 - 6213	1.45E-09	4	1.29E-09	3	4.12E-10	4	6.37E-10	1
Stimulations	4921 - 6213	1.66E-09	11	1.86E-09	10	5.60E-10	12	2.10E-10	1

[1] All data values included.
[2] Injection data with pump time >0.5 h.
[3] Recovery data with Horner time <1.5.

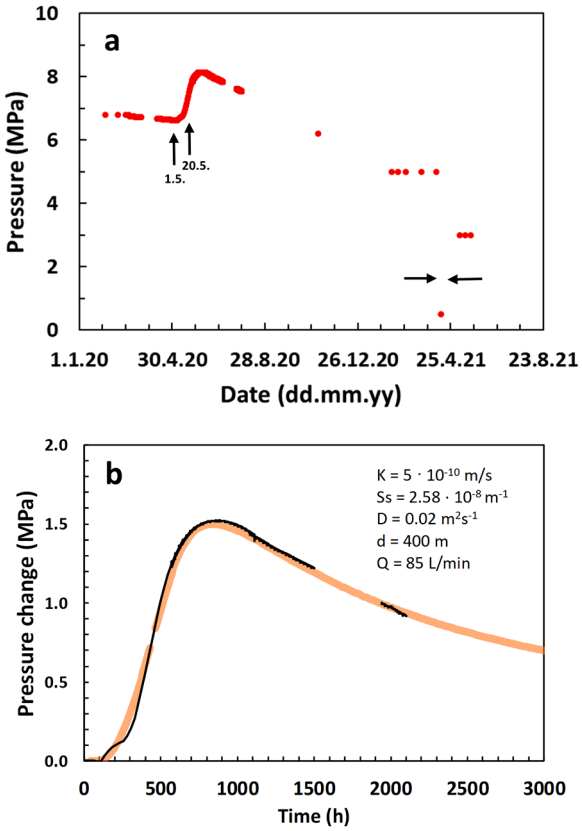

Fig. 8. a) OTN-3 shut-in pressures in 2020–2021. Readings before July 27, 2020 were digitally recorded, and thereafter the pressure readings were taken manually. Vertical arrows indicate begin (May 1, 2020) and end dates (May 20, 2020) of OTN-2 well testing and stimulation. Horizontal arrows indicate the period April 6 - 20, 2021, when OTN-3 was opened for pull out of seismic downhole instruments, and the hole was bleeding off. b) Modeling results of average hydraulic properties of rock mass between the wells derived from the pressure signal data. The black curves represent measured data and the thick orange curve the result calculated with the Theis model of an infinite confined aquifer.

7.3. The achieved reservoir: earthquake clusters and seismically reflecting zone

The spatio-temporal distribution of induced seismic events observed during the OTN-2 and OTN-3 stimulations was analyzed by Kwiatek et al. (2019) and Leonhardt et al. (2021) (Fig. 3). The stimulation yielded five different MEQ clusters, which show little spatial overlap (Fig. 3). Vertically the clusters are distributed over a depth range of 4.8 - 6.3 km TVD (Fig. 3). Further information on the reservoir structure was obtained from a VSP survey carried out in well OTN-3 in 2018 (Heikkinen et al., 2021). The VSP results revealed an ENE dipping (44°) reflecting zone, a structure (Fig. 9), which coincides with the weak rock zone encountered in deepening of OTN-3.

Logging data in OTN-3 and OTN-2 (Figs. 9–11) reveal the heterogeneous structure of the reflective zone. Lithological variation between granitic and metasedimentary/metavolcanic rocks (gneiss, amphibolite) occurs with layer thicknesses ranging from meters to hundreds of meters. Fractures are unevenly distributed, implying a reservoir which is hydraulically heterogeneous and consists of complicated fracture networks. This interpretation was supported by the hypocenter distribution of seismic events induced during the 2018 and 2020 stimulations, which indicated clustering of events spreading most often from the stimulation stages 1–3 in OTN-3 (Kwiatek et al., 2019). Taking into account the accuracy and resolution of hypocenter locations, it is conceivable that the main cluster of events may have spread from stimulation stage no. 2, which shows a distinct resistivity minimum (Fig. 10).

According to formation micro imager (FMI) logs in the OTN-3 open hole interval, fracture frequency is generally in the range of 0 - 4 m^{-1} with an average of 1.9 m^{-1} and maxima reaching 8 m^{-1}. The sections with high fracture frequencies are typically a few meters thick. Hydraulically conductive and partially conductive fractures as identified from minima in the FMI resistivity images (Fig. 10) represent only about 6% of the fractures. In OTN-2, FMI logs are not available, but downhole resistivity and sonic data suggest equally heterogeneous distribution of fractures, although the well was deviated to run along the seismic reflective structure (Figs. 10 and 11).

8. Discussion

8.1. Implications for hydraulic conductivity of crystalline rocks

Manning and Ingebritsen (1999) and Ingebritsen and Manning (1999) presented a model for the vertical variation of hydraulic permeability in the continental crust based on geothermal data and estimates of metamorphic fluid flow. In their model, permeability (k) decreases by about four orders of magnitude in the uppermost 10 km according to $\log k = -14 - 3.2 \log z$, where z is depth in km. At the brittle-ductile (B/D) transition and below in the crust (10–30 km depth), permeability converges towards a lower bound of about $5.0{\cdot}10^{-19}$ m^2. In the present Fennoscandian shield with low heat flow and geothermal gradient, the B/D transition is much deeper as indicated by the systematic cut-off depth of earthquakes at 28 ± 4 km (Veikkolainen et al., 2017). We note that the value predicted with the Ingebritsen and Manning (1999) model for 6.1 km is $3.1{\cdot}10^{-17}$ m^2. The values based on injection tests and shut-in data of OTN-3 ($9.8{\cdot}10^{-18}$ – $1.9{\cdot}10^{-16}$ m^2; Fig. 7a), and the cross-hole pressure data (conductivity $5{\cdot}10^{-10}$ m/s, permeability $1.4\ 0{\cdot}10^{-17}$ m^2; Fig. 8) are in a good agreement with the model. On the other hand, the well test results in OTN-2 (Fig. 7b) are lower and in the range of $5{\cdot}10^{-19}$ – $3{\cdot}10^{-17}$ m^2. The reason for this is not clear, but it may be due to the pressure dependence of conductivity, a pre-existing pressure field in the rock mass after the OTN-3 stimulation, or the geological structure deviating from the assumed homogeneous model assumed in Theis modeling. In general, we suggest that values of 10^{-18} – 10^{-17} m^2 are representative of the permeability at 5 – 6 km depth. Further, the average permeability at 6 – 28 km is most probably

Table 6
Wellhead pressures, closure pressures, net pressures and rock stress data in the OTN-3 well.

Operation	Wellhead pressure (MPa)	Hydrostatic pressure at 6.1 km (MPa)	Closure pressure at 6.1 km[1] (MPa)	Net pressure (MPa)	Stress S_H at 6.1 km[2] (MPa)	Stress S_V at 6.1 km[2] (MPa)	Stress S_h at 6.1 km[2] (MPa)	Azimuth of S_H[3] (°)
Stimulation injection	70.6 - 89.3	59.8	111.1 ± 3.4 (1 std)	18.5 - 37.2	230	167	100	109 ± 13
Stimulation recovery	61.8 - 89.3	59.8	111.1 ± 3.4 (1 std)	9.7 - 39.0	230	167	100	109 ± 13

[1] Closure pressures are from injection tets (Abbott, 2018).
[2] Stress data are estimated by extrapolation of the results of OTN-1 measurements at the depth range of 700 - 1720 m.
[3] Based on borehole break-outs in OTN-1 (Kukkonen, 2016).

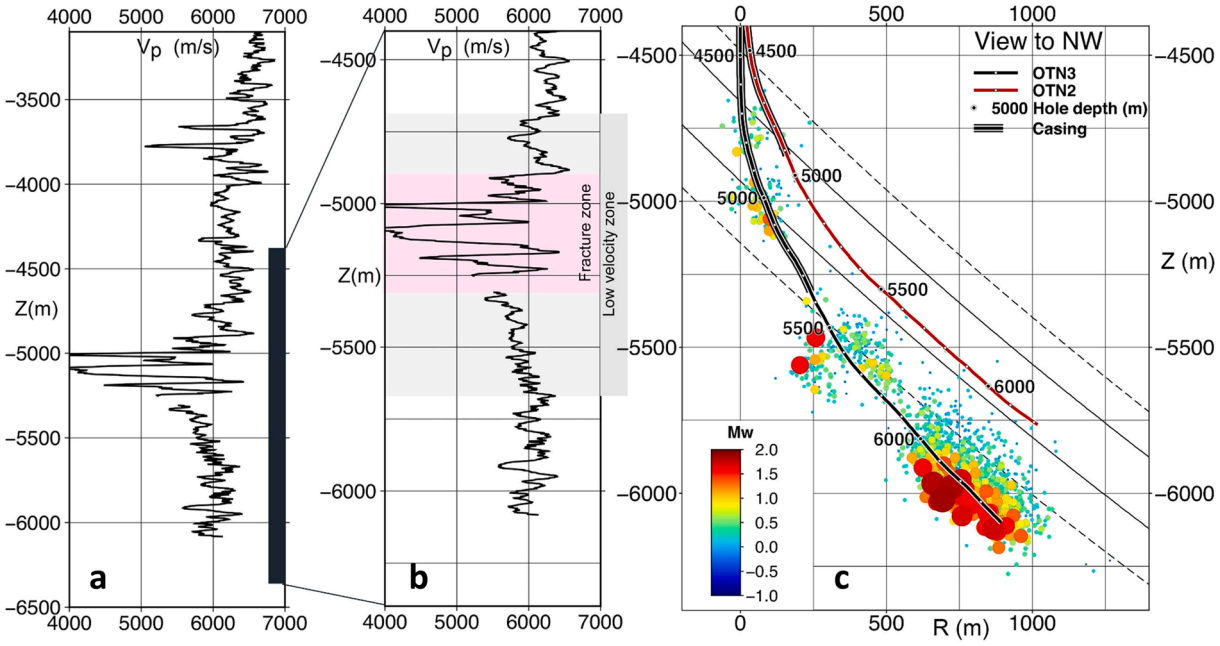

Fig. 9. a) P-wave velocity log compiled from sonic data in OTN-3a (from 3000 to 5250 m) and OTN-3c (beneath 5250 m). Depth is true vertical depth (TVD), b) Enlarged part of the P-wave velocity log corresponding to the depth range of the right panel, c) boundaries of the reflecting zone partially overlap with MEQ hypocenters of the 2018 and 2020 stimulations (from Leonhardt et al., 2021). Dashed lines show the boundaries of the low velocity zone, and the solid lines the heavily fractured zone, respectively. The location of the projection of panel c is indicated in Fig. 3.

in the range of 10^{-19} – 10^{-18} m^2, thus bracketed between our measured values and the ductile crust estimate by Manning and Ingebritsen (1999). Such permeabilities imply low values of thermal Peclet number in the Finnish shield conditions with low topographic variation and thus, low driving forces of flow (Kukkonen, 1995). Therefore, low natural flow rates and conductive heat transfer are expected to be dominant.

Bedrock temperature data, groundwater chemistry and characteristics of microbial life forms in fracture networks provide indirect evidence of hydraulic conductivity. Deep borehole thermal data, groundwater and dissolved gas chemistry and isotopes typically suggest very slow flow velocities and long residence times of fluids in the Finnish part of the Fennoscandian Shield (Nurmi et al., 1988; Kukkonen et al., 2011; Kietäväinen et al., 2013, 2014, 2017) and imply low levels of hydraulic conductivity. The hydraulic properties affect also the evolution and adaptation of the microbial life forms in fractured bedrock by controlling the fluid pathways and availability of energy and nutrients (Lin et al., 2006; Itävaara et al., 2011; Purkamo et al., 2016; Nuppunen-Puputti et al., 2020). These studies extending to about 2.5 km depth indicate stagnant waters with no significant exchange of fluids between different neighboring fracture systems or with surface waters (Kietäväinen et al., 2014). Noble gas residence times are in the range of 10 – 50 Ma. The stagnancy is enhanced by the density stratification of deep saline groundwater, which shows increasing salinity with depth. It is common in Fennoscandia (Nurmi et al., 1988; Smalley et al., 1988) and in other continental crystalline areas (Fritz and Frape, 1982; Bucher and Stober, 2000; Kloppmann et al., 2002; Frape et al., 2003). Free thermal convection is therefore unlikely in stable continental crust (Kukkonen, 1995). The situation may be different in tectonically active areas, orogenies and rift systems (Bataille et al., 2006; Ingebritsen and Manning, 2010).

Thermal logging data in the Siljan super-deep wells, central Sweden (Balling, 2013), exhibited spatially rapid local temperature gradient variations of ±20 mK/m at 1.5 – 3 km and 4.7 – 5 km on top of a stable gradient of 15 mK/m. Such variations are uncommon for shield conditions and most probably indicate flow in fractured rock. The Siljan bedrock can be exceptional as it was affected by a meteorite impact at 362 Ma (Bottomly et al., 1978), which may have opened fractures, and improved conductivity (Drake et al., 2019). On the other hand, the Kola superdeep hole revealed a vertical variation in geothermal gradient and heat flow in the uppermost 2 km (Arhavskaya et al., 1987; Popov et al., 1999), which cannot be attributed to steady-state conductive heat transfer. Thermal models of the Kola superdeep hole and the area (Kukkonen and Clauser 1994; Mottaghy et al., 2005), suggest the vertical variation in heat flow could be attributed to advective heat transfer due to the considerable topographic variation of the area (~400 m). Calibrated thermal models suggest hydraulic permeabilities in the range from 10^{-15} m^2 in the upper 2 km to 10^{-21} m^2 at 15 km (Kukkonen and Clauser, 1994; Mottaghy et al., 2005). However, paleoclimatic disturbances can also produce the observed vertical variation in heat flow in Fennoscandia and the East European platform (Kukkonen et al., 1998; Kukkonen and Joeleht, 2003), and the ground surface temperatures during the Weichselian glaciation may have been much lower than anticipated in previous modellings (Kukkonen et al., 1998; Glaznev et al., 2004; Demezhko et al., 2020). At the moment, there are no equilibrium temperature logs available of the OTN deep wells allowing permeability estimation via thermal models.

8.2. *Efficiency of stimulation in OTN-3 and OTN-2*

Interestingly, the stimulations of the two wells were accompanied by a transient enhancement of hydraulic conductivity; after shut-in, hydraulic conductivity returned to the initial values. The lack of significant permanent changes suggests that stimulation-induced irreversible deformation in the reservoir, as documented by the induced ~80,000 MEQs (Heikkinen et al., 2021), resulted only locally in self-propping of fractures and faults accompanied by permanent improvement of conductivity, if at all. The pre-existing fractures intersecting the boreholes and establishing the hydraulic connection to the bulk reservoir appear to have opened and closed almost elastically. Their ubiquity hindered the formation of new fractures at the borehole walls. The formation's structural and hydraulic heterogeneity might have limited the efficiency of the stimulations, as evidenced by the distribution of MEQ clusters related to OTN-3 and OTN-2 stimulations. Several spatially poorly overlapping clusters were generated instead of one that would connect

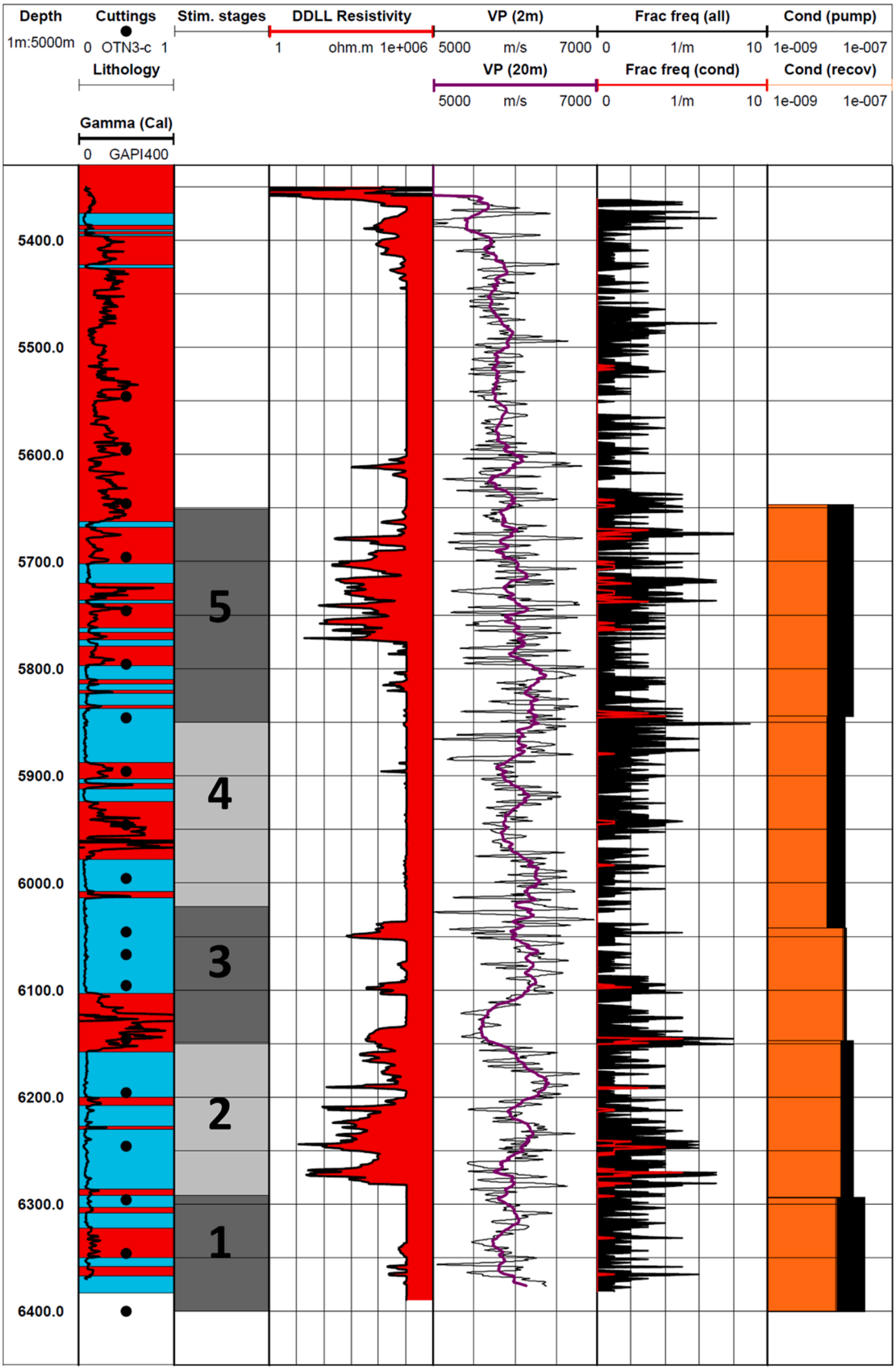

Fig. 10. Selection of OTN-3c pre-stimulation logging data at 5.3–6.4 km MD depth. From left: Gamma, cutting sample depths (black dots), lithology (red, granitic; blue, metasediments), stimulation stages 1 – 5, rock resistivity, V_P logs with 2 m and 20 m moving averages, fracturing from FMI log, average hydraulic conductivities of stimulation stages during pumping (black) and recovery (orange). Depth intervals of 2018 stimulation stages are shown in shades of gray (numbers 1–5, Table 4). DDLL resistivity implies remarkable differences in fracturing between different stimulation intervals. P-velocity shows correlation with lithologies and fracturing.

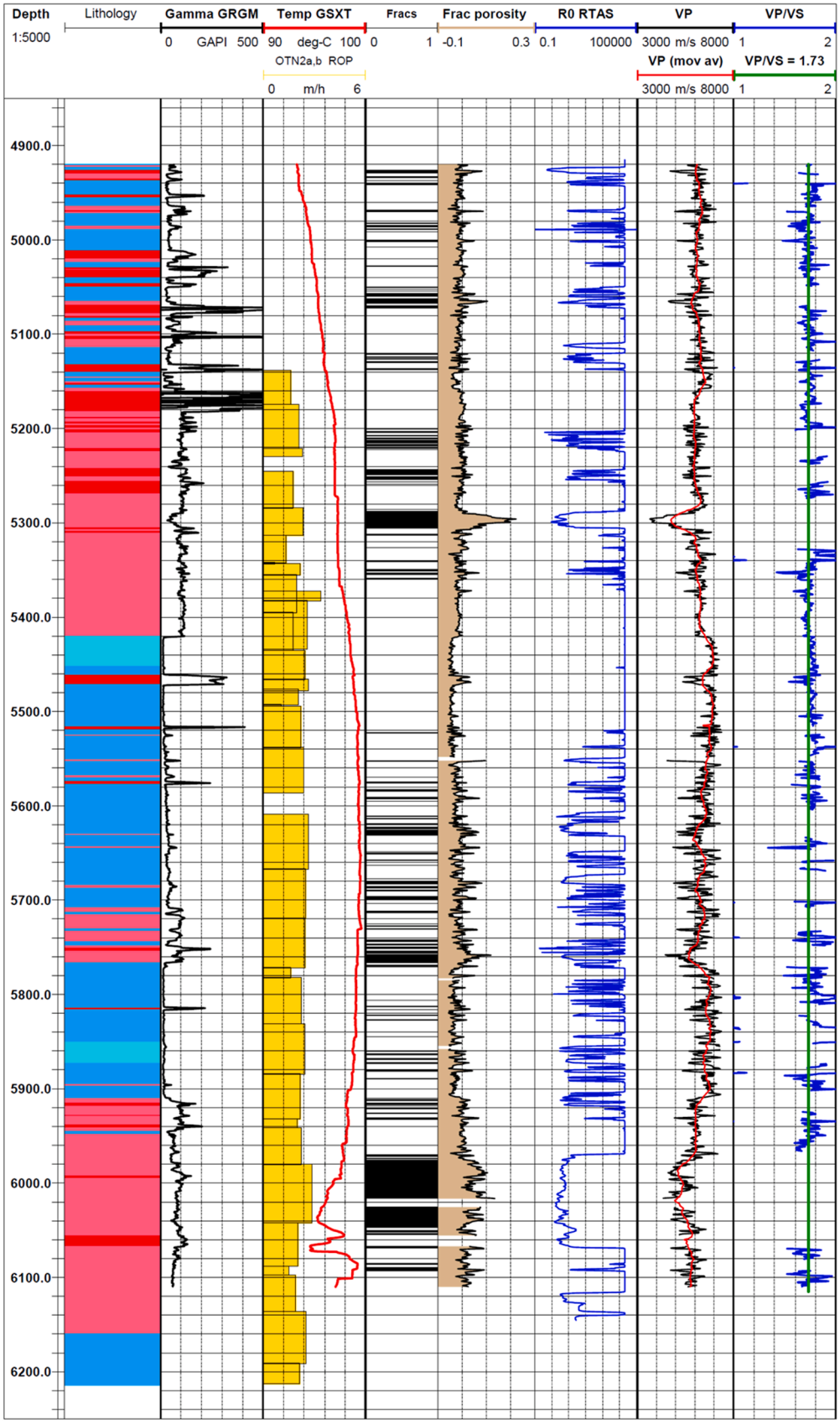

Fig. 11. Selection of OTN-2 pre-stimulation logging data. From left: Gamma, lithology, rate of penetration in drilling (ROP), temperature, fracturing intervals estimated from sonic and resistivity, rock resistivity, fracture porosity estimated from sonic, V_P (measured data and 20 m moving average) and V_P/V_S ratio. The complete open hole section 4.9 – 6.2 km MD was stimulated as one interval. Fracturing estimated from resistivity and sonic logs implies heterogeneous distribution of fractures in the reservoir. Temperature log shows an isothermal section at 5.5 – 6.0 km MD which is attributed to flow between the well and formation.

the two wells (Fig. 3).

Stimulation of well OTN-2 resulted in a seismic event distribution spreading to the NE of the well (Fig. 3) in contrast to the MEQ clusters stimulated in OTN-3 that was mostly centered around the well. This disparity in cloud spreading may, in addition to natural directional variations in hydraulic conductivity, be partly related to the pressure field generated by the stimulation in OTN-3 two years earlier, which had not attenuated by the time of the OTN-2 stimulation. According to Theis modeling, there may have been an overpressure of about 2 – 4 MPa at the location of OTN-2 (distance ca. 400 m from OTN-3). Although small in comparison to stimulation pressures, it may have influenced the build-up of pressures from OTN-2. As a result, the new pressure field was not built symmetrically around OTN-2 but it was forced to NE.

Significant formation of break-outs and washouts occurred at the end of drilling of OTN-3, when the heavy drilling mud was replaced with fresh water. Logging data indicate the caliper of the well increased from the nominal of 8.5″ (216 mm) to values locally as high as 17″ (432 mm). The placing of the packers was therefore strongly constrained by the few available sections where packers could be assumed to work properly. We cannot be sure that the rock was intact at sections where packers were installed, and leakage via bedrock is possible. Leakage from nominally isolated intervals may have contributed to the spatial characteristics of event clusters. This observation underlines how difficult stimulation operations can be in crystalline rock under high stress.

The St1 stimulations were controlled with two parameters, a pre-set wellhead pressure (70 – 90 MPa) and the TLS with an earthquake magnitude limit (red M2.1) (Kwiatek et al., 2019; Ader et al., 2019), which were not to be exceeded. With the available pumps, the flow rates could be controlled only at steps of 0.2 m^3/min. Therefore, pumping was carried out cyclically in OTN-2 with pump periods of about 1 hour followed by recovery periods of 2 h to stay below the pressure limit. The applied periodicity resulted in a gradual increase of the starting levels of pressure from one pumping period to the next (Fig. 12). We interpret this as an indication of gradual pressurization of the near-wellbore volume. Fluid injected at later cycles encountered a high-pressure annulus, which hampered the flow of the fluid further out from the well. An alternative to counter this successive pressure increase could be stimulation with a much lower flow rate, but longer injection times.

8.3. Outlook for EGS in crystalline rocks

Achieving the required high temperature is not a critical risk in an EGS. Temperatures are rather accurately estimated for 5 – 6 km depths with standard thermal models. Drilling to such depths is not an insurmountable technological challenge either, although difficult rock conditions may increase drilling time and cost, but hydraulic conductivity and achieving economically viable flow rates are much more challenging, as shown in many EGS projects (Olasolo et al., 2016; Lu, 2018). Natural conductivity is usually insufficient for EGS thermal power production, and engineering of conductivity is necessary. Hydraulic conductivity should be high ($\sim 10^{-8}$ – 10^{-7} m/s) and homogeneous over a sufficiently large rock volume ($\sim$ 0.3 – 1 km^3) to allow economic extraction of heat from the reservoir for decades. However, in fractured crystalline rock, flow may be directed through high-conductivity pathways resulting in thermal breakthrough and early cooling of the production fluid (e.g., Parker, 1999).

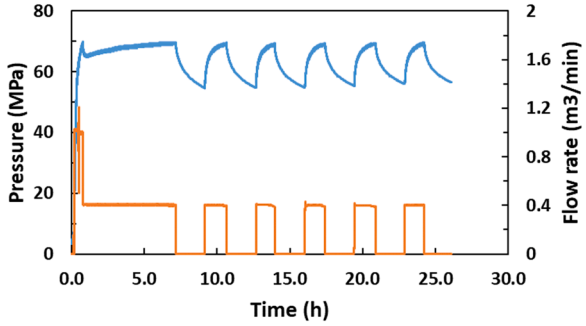

Fig. 12. OTN-2 stimulation stage 10 flow rates (orange line) and pressures (blue line) with 1 h pumping periods followed by 2 h recovery periods. Maximum allowed wellhead pressure was 70 MPa. Pressure did not relax below 55 MPa after pumping, and the starting level of pressure increased about 3 MPa/cycle (red dashed line), leaving a gradually narrowing marginal for pumping operations.

Stimulation of a heterogeneous fractured medium produces flow into structures of lowest resistance, i.e., existing fractures, and new fractures are not necessarily formed. Pressure diffusion from a stimulation interval attenuates rapidly with distance, and it is practically impossible to create new fractures at distances of few hundred meters. However, only small overpressures are required to activate critically stressed pre-existing fractures (Ito and Zoback, 2000), which is evidenced by the generated seismicity in the present study as well as elsewhere (Holl and Barton, 2015; Hogarth and Holl, 2017). Stimulation influences especially the near-drillhole space. With long borehole distances, it becomes difficult to predict the result of a stimulation. Typically, stimulation can increase the productivity of a well by 1–2 orders of magnitude at best (Smith and Shlyapobersky, 2000; Schill et al., 2017; Hofmann et al., 2019, 2021).

Rock conductivity is proportional to the third power of fracture width. Thus, increasing the fracture width is a major aim in stimulation. Further, the fracture width is proportional to pump rate and fluid viscosity (Smith and Shlyapobersky, 2000). There is a limit for increasing the aperture by overpressure, as stimulation pressures (at wellhead) are limited due to technical and economic reasons and their implications for induced seismicity. A solution for this problem could be applying short stimulation depth intervals allowing focusing of the pressure effect in the formation. An alternative could be either slow injection of fluid over longer injection periods or the so-called soft stimulation with short injection periods but gradually increasing flow rates (Zang et al., 2013; Huenges et al., 2018, 2013, 2019; Hofmann et al., 2021). Cyclically varying pump rate is expected to produce fatigue in the rock resulting in more gradual fracture propagation and a smaller damage volume. According to a field scale 2D discrete element modeling of conventional (i.e., constant flow rate) and soft stimulation (Zang et al., 2013), the induced seismicity event numbers and magnitudes decrease in soft stimulation, and the final achieved permeability enhancement is about 12% better than in conventional stimulation. However, such results have not been demonstrated in practice. In the present study, the flow rates were also varied in a cyclic manner, but it is not possible to estimate any benefit of the cyclic stimulation to permeability as no conventional stimulation was carried out.

By manipulation of the viscosity of the stimulation fluid, it is possible to decrease hydraulic impedance (Smith and Shlyapobersky, 2000). Using supercritical CO_2 as the EGS working fluid instead of water would allow higher flow and heat extraction rates due to lower viscosity of CO_2 (Brown, 2000). Modeling suggests supercritical CO_2 would provide better heat extraction rates by a factor of about two, and the effect is higher in low-temperature reservoirs (Pruess, 2006).

The concept of an Enhanced Geothermal System evolved from the original HDR concept (Brown et al., 2000) based on generating an artificially fractured confined reservoir in intact crystalline rock. Difficulties in stimulating new fractures in naturally fractured media led to concepts using existing fractures and permeable alteration zones favorably oriented with the prevailing stress field (Ledesert et al., 2010; Olasolo et al., 2016; Schill et al., 2017; Hogarth and Holl, 2017; Lu, 2018). More recently, crustal fault zones have been targets in EGS exploration (Duwiquet et al., 2021; Schmittbuhl et al., 2021). These targets imply that the stimulated reservoir will not be confined and the system will largely, if not completely, depend on natural conductivity and its enhancement, as well as becoming prone to uncontrolled induced seismicity (Häring et al., 2008; Grigoli et al., 2018; Kim et al., 2018;

Schmittbuhl et al., 2021). The concept of an EGS heat exchanger consisting of two boreholes with injection and production intervals at a distance of a few hundred meters is not site-independent and applicable anywhere. Instead, it heavily depends on the local geological conditions and requires extensive subsurface surveys and operations to achieve economically viable and sustainable energy production.

Many problems of EGS are related to the great depths of wells required to reach sufficient temperatures. In a shield setting, as in the present St1 case, the boreholes had to be deep. The great depth brings along the problems of high stresses, which makes the technical borehole conditions difficult. Particular attention should be paid to the borehole completion and its influence for successful stimulation. A major reservoir challenge is the elastic response of the fractured rock to stimulation, which resets the achieved enhancement in conductivity. High stresses complicate the use of proppants for keeping the fractures open (Bortolan Neto et al., 2015; Man and Wong, 2017; Chen et al., 2021). In the St1 project, it was estimated that typical ceramic proppants would be either crushed or embedded into rock, which could worsen the hydraulic situation. However, to overcome the problem of elastic closure of fractures, proppants seem to be the best option.

It is obvious that stimulation in a hydraulically heterogeneous fractured medium is not predictable in detail, in particular if the stimulation stages are long. Flow will undoubtedly become channeled through high-conductivity fractures, resulting in less efficient overall stimulation. Currently, the only means to overcome these problems would be application of shorter stimulation intervals, and shorter borehole distances and developing proppant technologies applicable at high rock stress. Redesign of the EGS borehole configuration geometry is required. Leary et al. (2014) suggested drilling several parallel production wells at short distances around a central lateral injection well. Stimulation of the injection well produces a high permeability wellbore-centric annulus that can act as a permeable volume. Such models can provide a roadmap for site-independent engineering of EGS.

9. Conclusions

The St1 Deep Heat Project successfully drilled two deep wells to 6 km depth level in crystalline rock. The hydraulic stimulation results provided direct observations of hydraulic conductivity at depths rarely tested with in situ measurements. Hydraulic conductivity was observed to be pressure-dependent, heterogeneous and affected by fracturing and lithological variation. Only a small fraction of the natural fractures were open and conductive, resulting in a hydraulically heterogeneous medium. The average natural hydraulic conductivity derived from leak-off tests and well tests (in OTN-3) before stimulation and from cross-hole pressure data is of the order of $5{\cdot}10^{-10}$ – $5{\cdot}10^{-9}$ m/s (permeability $1.4{\cdot}10^{-17}$ – $1.4{\cdot}10^{-16}$ m^2), which is in agreement with previous generalizations of brittle crystalline crust permeability models for 6 km depth. At levels deeper than 6 km, down to the brittle-ductile transition, hydraulic permeability is most probably in the range 10^{-17} – 10^{-19} m^2. Hydraulic stimulation increased conductivity to 10^{-8} – 10^{-7} m/s level, but due to the elastic response of the fractured medium, conductivity values gradually decreased back to levels close to natural after relaxation of pressure. Proppants were not be used due to high stresses. Stimulation generated five micro-earthquake clusters at 4.8 – 6.3 km TVD depth. Hydraulic connections between clusters were not effectively attained due to heterogeneous conductivity.

Generally, the project demonstrated that rock temperatures sufficient for district heating purposes can be attained at the depth of 6 km in southern Finland. Further, the project carried out two stimulation campaigns at depth with considerable volumes (7000 – 18,000 m^3) of injection fluid. Stimulation did not result in seismic events exceeding the earthquake magnitude limit (M_L2.1) set by regulating authorities, an encouraging signal for developing EGS methods and technologies for sustainable thermal power production in other shield areas. The St1 project generated extensive experience and data sets of the continental crust, deep drilling, hydrogeological properties and seismic response of the crystalline rock to stimulation. Hydraulic conductivity was found to be the most challenging issue for EGS development and the St1 EGS project is not continued at present. Proceeding towards economically and technically more viable and universally applicable EGS in fractured high-stress crystalline rock environments calls for further development of stimulation techniques and re-design of heat exchanger borehole geometries.

CRediT authorship contribution statement

Ilmo Kukkonen: Conceptualization, Investigation, Methodology, Visualization, Writing – original draft, Writing – review and editing. **Pekka Heikkinen**: Seismicity, VSP and SWD analysis, Visualization, Writing. **Peter Malin**: Seismicity, Writing – review and editing. **Joerg Renner**: Investigation, Writing – review and editing. **Georg Dresen**: Visualization, Writing – review and editing. **Aino Karjalainen**: Data curation, Writing – review and editing. **Jussi Rytkönen**: Data curation, Investigation, Writing – review and editing. **Juha Solantie**: Project administration, Writing – review and editing.

Declaration of Competing Interest

The authors declare that they have no known competing financial interests or personal relationships that could have appeared to influence the work reported in this paper.

Data availability

The stimulation data of OTN-3 and OTN-2 wells are provided in the supplementary material, https://data.mendeley.com/datasets/ycdcw2rdfj/1.

Acknowledgements

We are grateful to St1 for permission to use and publish the stimulation data. Chris Juhlin and an anonymous reviewer helped in improving the manuscript.

References

Abbott, J., 2018. St1 Injection and Closure Analysis. Schlumberger, report to St1 10. June 2018.

Arhavskaya, N., Galdin, N., Karus, E., Kuznetsov, O., Lubimova, E., Milanovsky, S.Y., Nartikoev, V.D., Semashko, S.A., Smirnova, E.V., 1987. Geothermic investigations. In: Kozlovsky, Y.A. (Ed.), The Superdeep Well of the Kola Peninsula. Springer, Berlin, pp. 387–394.

Ader, T., Chendorain, M., Free, M., Saarno, T., Heikkinen, P., Malin, P.E., Leary, P., Kwiatek, G., 2019. Design and implementation of a traffic light system for deep geothermal well stimulation in Finland. J. Seismolog. https://doi.org/10.1007/s10950-019-09853-y 2019. ISSN 1383-4649 J Seismol.

Ahonen, L., Kietäväinen. R., Kortelainen, N., Kukkonen, I.T., Pullinen, A., Toppi, T., Bomberg, M., Itävaara, M., Nousiainen, A., Nyyssönen, M., Öster, M., 2011. Hydrological characteristics of the Outokumpu deep drill hole, In: Outokumpu Deep Drilling Project, Kukkonen I.T. (ed), Finnish Geological Survey (GTK) Special Paper 51, pp 151–168.

Airaksinen, J.U., 1978. Maa – Ja Pohjavesihydrologia. Kustannusyhtiö Pohjoinen, Oulu, p. 248.

Backers, T. and Meier, T., 2016. Stress field modeling for the planned St1 Deep Heat geothermal wells for Aalto University, Finland. Geomecon GmbH, Report A1601/St1/160508fr, 41 p.

Balling, N., 2013. Doctoral dissertation. Aarhus University, Denmark, p. 195.

Banks, D., Odling, N.E., Skarphagen, H., Rohr-Torp, E., 1996. Permeability and stress in crystalline rocks. Terra Nova 8, 223–235, 1996.

Bataillé, A., Genthon, P., Rabinowicz, M., Fritz, B., 2006. Modeling the coupling between free and forced convection in a vertical permeable slot: implications for the heat production of an Enhanced Geothermal System. Geothermics 35, 654–682.

Bear, J., 1979. Hydraulics of Groundwater. McGraw-Hill, New York, p. 569.

Becker, F., 2015. EGS Heat Plant Project Otaniemi/Finland, hydraulic fracturing stress measurements in borehole OTN-1. MeSy-Solexperts GmbH, Bochum, Germany, Report DE-1077, 13 p.

Borevsky, L.V., Vartanyan, G.S., Kulikov, T.B., 1987. Hydrological essay. In: Kozlovsky (Ed.), The Superdeep Well of the Kola Peninsula. Springer, pp. 271–287.
Bortolan Neto, L. Khanna, A., and Kotousov, A., 2015. Conductivity and performance of hydraulic fractures partially filled with compressible proppant packs. Int. J. Rock Mech. Min. Sci. 74 (2015),1–9. doi:10.1016/j.ijrmms.2014.11.005.
Bottomly, R.J., York, D., Grieve, R.A.F., 1978. Ar-Ar ages of Scandinavian impact structures: i Mien and Siljan. Contrib. Mineral Petrol 68, 79–84.
Brace, W.F., 1984. Permeability of crystalline rocks: new in situ measurements. J. Geophys. Res. 89, 4327–4330.
Brown, D.W., 2000. A hot dry rock geothermal energy concept utilizing supercritical CO2 instead of water. In: Pcoceedings, Twenty-Fifth Workshop on Geothermal Reservoir Engineering. Stanford University, Stanford, California. January 24-26, 2000, SGP-TR-165.
Brown, D.W., Duchane, D.V., Heiken, G., Hriscu, V.T., 2000. Mining the Earth's heat: Hot dry Rock Geothermal Energy. Springer, Berlin, p. 655.
Bucher, K., Stober, I., 2000. The composition of groundwater in the continental crystalline crust. In: Stober, I., Bucher, K. (Eds.), Hydrogeology of Crystalline Rocks. Kluwer, Dordrecht, pp. 141–176.
Chen, T., Fu, Y., Feng, X.-T., Tan, Y., Cui, G., Elsworth, D., and Pan., Z., 2021. Gas permeability and fracture compressibility for proppant-supported shale fractures under high stress. J Nat Gas Sci Eng; 95 (2021), 104157. doi:10.1016/j.jngse.2021.104157.
Clauser, C., 1992. Permeability of crystalline rocks. EOS, Trans. Am. Geopys. Un., 73, 233–237.
Demezhko, D.Yu., Gornostaeva, A.A., Antipin, A.N., 2020. The Fennoscandian ice sheet during the Late Weichselian: geothermal evidence. Int. J. Earth Sci. https://doi.org/10.1007/s00531-020-01881-1.
Domenico, P.A., Schwartz, F.W., 1998. Physical and Chemical Hydrogeology, 2n ed. John Wiley & Sons, Chichester, p. 506.
Drake, H., Roberts, N.M.W., Heim, C., Whitehouse, M.J., Siljeström, S., Kooijman, E., Broman, C., Ivarsson, M., Åström, M.E., 2019. Timing and origin of natural gas accumulation in the Siljan impact structure, Sweden. Nature Comm. 10, 4736. https://doi.org/10.1038/s41467-019-12728-y.
Duwiquet, H., Guillou-Frotti, L., Arbaret, L., Bellanger, M., Guillon, T., Heap, M.J., 2021. Crustal Fault Zones (CFZ) as Geothermal Power Systems: a Preliminary 3D THM Model Constrained by a Multidisciplinary Approacher. Geofluids 2021, 8855632. https://doi.org/10.1155/2021/8855632. Article IDpages.
Economides, M.J., Nolte, K.G., 2000. Reservoir Stimulation. John Wiley & Sons, Chichester.
Ehlig-Economides, C., 1988. Use of the Pressure Derivative for Diagnosing Pressure-Transient Behavior. J. Petrol. Technol. 1280–1282. October 1988.
Frape S.K., Blyth A., Blomqvist R., McNutt R.H. and Gascoyne, M., 2003. Deep fluids in the continents: II. Crystalline rocks. In: Drever, J. I. (ed.), Surface and Ground water, Weathering and Soils. Treatise Geochem. 5, 541–580.
Fritz, P., Frape, S.K., 1982. Saline groundwaters in the Canadian Shield—a first overview. Chem. Geol. 36, 179–190.
Glaznev, V.N., Kukkonen, I.T., Raevsky, A.B., Jokinen, J., 2004. Novye dannye o teplovom potoke v zentralnoy chasty Kolskogo Polyostrova. Dokl. Acad. Nauk 396, 102–104 in Russian.
Grigoli, F., Cesca, S., Rinaldi, A.P., Manconi, A., Lopez-Comino, J.A., Clinton, J.F., Westaway, R., Cauzzi, C., Dahm, T., Wiemer, S., 2018. The November 2017 MW 5.5. Pohang earthquake: a possible case of induced seismicity in South Korea. Science. https://doi.org/10.1126/science.aat2010(2018).
Guljarani, S.N., Nolte, K.G., 2000. Fracture evaluation using pressure diagnostics. In: Economides, M.J., Nolte, K.G. (Eds.), Reservoir Stimulation. John Wiley & Sons, Chichester, pp. 9.1–9.63.
Häring, M.O., Schanz, U., Ladner, F., Dyer, B.C., 2008. Characterisation of the Basel 1 enhanced geothermal system. Geothermics 37 (2008), 469–495.
Heikkinen, P., Giese, R., Kueck, J., Kukkonen, I., Malin, P., 2021. Basement-EGS Structure from VSP, Drilling, Well Logs, and Geology in Espoo. Finland. GRC Transactions 45. https://publications.mygeoenergynow.org/grc/1034472.pdf.
Hillers, G., Vuorinen, T.A.T., Uski, M.R., Kortström, J.T., Mäntyniemi, P.B., Tiira, T., Malin, P.E., Saarno, T., 2020. The 2018 geothermal reservoir stimulation in Espoo/Helsinki, Southern Finland: seismic network anatomy and data features. Seismol. Res. Lett. 91, 770–786.
Hofmann, H., Zimmermann, G., Farkas, M., Huenges, E., Zang, A., Leonhardt, M., et al., 2019. First field application of cyclic soft stimulation at the Pohang Enhanced Geothermal System site in Korea. Geophys. J. Int. 217 (2), 926–949. https://doi.org/10.1093/gji/ggz058.
Hofmann, H., Zimmermann, G., Huenges, E., Regenspurg, S., Aldaz, S., Milkereit, C., Heimann, S., Dahm, T., Zang, A., Grigoli, F., Karvounis, D., Broccardo, M., Wiemer, S., Hjörleifsdottir, V., Kristjansson, B.R., Hersir, G.P., Asgeirsdottir, R.St., Magnússon, R., Arnadottir, S., 2021. Soft stimulation treatment of geothermal well RV-43 to meet the growing heat demand of Reykjavik. Geothermics 96 (2021), 102146.
Hogarth, R., Holl, H.-.G., 2017. Lessons learnt from the Habanero EGS project. GRC Transactions 41 (2017), 13.
Holl, H.-.G., Barton, C., 2015. Habanero field – Structure and state of stress. In: Proceedings World Geothermal Congress 2015. Melbourne, Australia, p. 8, 19-25 April 2015.
Huenges, E., Erzinger, J., Kueck, J., Engeser, B., Kessels, W., 1997. The permeable crust: geohydraulic properties down to 9101m depth. J. Geophys. Res. 102, 18.255–18.265. GRC Transactions, Vol. 42, 2018.
Huenges, E., Ellis, J., Hofmann, H., Zimmermann, G., Brehme, M., Farkas, M., Nowak, K., Westaway, R., Burnside, N., Min, K.-.B., Yoon, K., Genter, A., Guinot, F., Marti, M., 2018. Concepts of soft stimulation treatments in geothermal reservoirs. GRC Transactions 42, 14.
Ingebritsen, S.E., Manning, C.E., 1999. Geological implications of a permeability-depth curve for the continental crust. Geology 27, 1107–1110.
Ingebritsen, S.E., Manning, C.E., 2010. Permeability of the continental crust: dynamic variations inferred from seismicity and metamorphism. Geofluids 10, 193–205, 10.1111.
Itävaara, M., Nyyssönen, M., Bomberg, M., Kapanen, A., Nousiainen, A., Ahonen, L., Hultman, J., Paulin, L., Auvinen, P., Kukkonen, I.T., 2011. Microbiological sampling and analysis of the Outokumpu Deep Drill Hole biosphere in 2007-2009. In: Kukkonen, I.T. (Ed.), Outokumpu Deep Drilling Project 2003-2010. Geological Survey of Finland, pp. 199–206. Special Paper 51.
Ito, T., Zoback, M.D., 2000. Fracture permeability and in situ stress to 7km depth in the KTB scientific drillhole. Geophys. Res. Lett. 27, 1045–1048.
Juhlin, C. (Ed.), 1991. Scientific summary report of the Deep Gas Drilling Project in the Siljan Ring impact structure. Vattenfall Co., report U(G) 1991/14, 278 p.
Kietäväinen, R., Ahonen, L., Kukkonen, I.T., Hendriksson, N., Nyyssönen, M., Itävaara, M., 2013. Characterisation and isotopic evolution of saline waters of the Outokumpu Deep Drill Hole, Finland – Implications for water origin and deep terrestrial biosphere. Appl. Geochem. 32, 37–51. https://doi.org/10.1016/j.apgeochem.22012.10.013.
Kietäväinen, R., Ahonen, L., Kukkonen, I.T., Niedermann, S., Wiersberg, T., 2014. Noble gas residence times of saline waters within crystalline bedrock, Outokumpu Deep Drill Hole, Finland. Geochim. Cosmochim. Acta 145, 159–174.
Kietäväinen, R., Ahonen, L., Niinikoski, P., Nykänen, H., Kukkonen, I.T., 2017. Abiotic and biotic controls on methane formation down to 2.5km depth within the Precambrian Fennoscandian Shield. Geochemica Cosmochimica Acta 202, 124–145.
Kim, K.-H., Ree, J.-H., Kim, Y.H., Kim, S., Kang, S.Y., Seo, W., 2018. Assessing whether the 2017 Mw 5.4 Pohang earthquake in South Korea was an induced event. ScienceScience 360, 1007–1009.
Kloppmann, W., Girard, J.-P., Négrel, P., 2002. Exotic stable isotope compositions of saline waters and brines from the crystalline basement. Chem. Geol. 184, 49–70.
Kozlovsky, Ye.A., 1987. The Superdeep Well of the Kola Peninsula. Springer, Berlin, p. 558.
Kukkonen, I.T., 1995. Thermal aspects of groundwater circulation in bedrock and its effect on crustal geothermal modelling in Finland, the central Fennoscandian Shield. Tectonophysics 244, 119–136.
Kukkonen, I.T., 2011. Outokumpu Deep Drilling Project 2003-2010. Geological Survey of Finland 252. Special Paper 51.
Kukkonen, I.T., 2016. Stress field direction in Otaniemi OTN-1 borehole. Report to St1, 12 p.
Kukkonen, I.T., Clauser, C., 1994. Simulation of heat transfer at the Kola deep-hole site - implications for advection, heat refraction and paleoclimatic effects. Geophys. J. Int. 116, 409–420.
Kukkonen, I.T., Jõeleht, 2003. Weichselian temperatures from geothermal heat flow data. J. Geophys. Res. 108 (B3), 11. ETG-9.
Kukkonen, I.T., Gosnold, W.D., Šafanda, J., 1998. Anomalously low heat flow density in eastern Karelia, Baltic Shield: a possible palaeoclimatic signature. Tectonophysics 291, 235–249.
Kukkonen, I.T., Rath, V., Kivekäs, L., Safanda, J., Cermak, V., 2011. Geothermal studies of the Outokumpu Deep Drill Hole, Finland: vertical variation in heat flow and palaeoclimatic implications. Phys. Earth Planet. Inter. 188 (1–2), 9–25.
Kwiatek, G., Saarno, T., Ader, T., Bluemle, F., Bohnhoff, M., Chendorain, M., Dresen, G., Heikkinen, P., Kukkonen, I., Leary, P., Leonhardt, M., Malin, P., Martínez-Garzón, P., Passmore, K., Passmore, P., Valenzuela, S., Wollin, C., 2019. Controlling fluid-induced seismicity during a 6.1-km-deep geothermal stimulation in Finland. Sci. Adv. 5, eaav7224. https://doi.org/10.1126/sciadv.aav7224.
Leary, P., Malin, P., Pogacnik, J., Valles, B., Geiser, P., 2014. Lognormality, $\delta\kappa \sim \kappa\, \delta\varphi$, EGS, and All That. In: Proc. Thirty-Ninth Workshop on. Stanford, California. Geothermal Reservoir Engineering Stanford University. February 24-26, 2014 SGP-TR-202.
Ledesert, B., Hebert, R., Genter, A., Bartier, D., Clauer, N., Grall, C., 2010. Fractures, hydrothermal alterations and permeability in the Soultz Enhanced Geothermal System. Collect C R Geosci 342, 607–615.
Leonhardt, M., Kwiatek, G., Martínez-Garzón, P., Bohnhoff, M., Saarno, T., Heikkinen, P., Dresen, G., 2021. Seismicity During and After Stimulation of a 6.1Km Deep Enhanced Geothermal System in Helsinki. EGU Solid Earth, Finland. https://doi.org/10.5194/se-2020-139.2020.
Lin, L.-H., Wang, P.-L., Rumble, D., Lippmann-Pipke, J., Boice, E., Pratt, L.M., Sherwood Lollar, B., Brodie, E.L., Hazen, T.C., Andersen, G.L., DeSantis, T.Z., Moser, D.P., Kershaw, D., Onstott, T.C., 2006. Long-term sustainability of a high-energy, low-diversity crustal biome. ScienceScience 314, 479–482.
Lu, S.-M., 2018. A global review of enhanced geothermal system (EGS). Renewable Sustainable Energy Rev. 81, 2902–2921.
Mäkelä, J., 2012. Doctoral thesis. University of Turku, Ann. Univ. Turkuensis, p. 267.
Malin, P.E., Leary, P.C., Cathles, L.M., Barton, C.C., 2020. Observational and Critical State Physics Descriptions of Long-Range Flow Structures. Geosciences (Basel) 2020 (10), 50. https://doi.org/10.3390/geosciences10020050.
Manning, C.E., Ingebritsen, S.E., 1999. Permeability if the continental crust: implications of geothermal data and metamorphic systems. Rev Geophys 37, 127–150.
Man, S. and Wong, C.-K., 2017. Compression and crushing behavior of ceramic proppants and sand under high stresses. J. Pet. Sci. Eng. 158 (2017) 268–283. doi:10.1016/j.petrol.2017.08.052.
McEwen, T. and Äikäs, T., 2000. The site selection process for a spent fuel repository in Finland - Summary report. Posiva Oy (Finland), Report POSIVA 2005-15, 224 p.

Mottaghy, D., Schellschmidt, R., Popov, Yu.A., Clauser, C., Kukkonen, I.T., Nover, G., Milanovsky, S., Romushkevich, R.A., 2005. New heat flow data from the immediate vicinity of the Kola super-deep borehole: vertical variation in heat flow confirmed and attributed to advection. Tectonophysics 401, 119–142.

Nuppunen-Puputti, M., Kietäväinen, R., Purkamo, L., Rajala, P., Itävaara, M., Kukkonen, I., Bomberg, M., 2020. Rock Surface Fungi in Deep Continental Biosphere—Exploration of Microbial Community Formation with Subsurface In Situ Biofilm Trap. Microorganisms 2021 (9), 64. https://doi.org/10.3390/microorganisms9010064.

Nurmi, P., Kukkonen, I., Lahermo, P., 1988. Geochemistry and origin of saline ground–waters in the Fennoscandian Shield. Appl. Geochem. 3, 185–203.

Olasolo, P., Juárez, M.C., Morales, M.P., D'Amico, S., Liarte, I.A., 2016. Enhanced geothermal systems(EGS): a review. Renewable Sustainable Energy Rev. 56, 133–144.

Ortiz, A.E., Renner, J., Jung, R., 2011. Hydromechanical analyses of the hydraulic stimulation of borehole Basel 1. Geophys. J. Int. 185 (2011), 1266–1287.

Pajunen, M., 2008. Tectonic evolution of the Svecofennian crust in southern Finland – a basis for characterizing bedrock technical properties. Geological Survey of Finland 326. Special Paper 47p.

Palmén, J., , Vaittinen, T., Ahokas, H., Nummela. J. and Heikkinen, E., 2004. 3D-model of salinity of bedrock groundwater at Olkiluoto. Working report 2004-53, Posiva Oy, Finland, 92 p.

Parker, R., 1999. The Rosemanowes HDR project 1983 –1991. Geothermics 28, 603–615.

Pitkänen, P., Snellman, M., Leino-Forsman, H., Front, K., 1992. Groundwater chemistry and water-rock interaction at Olkiluoto. Report YJT-92-02, Nuclear Waste Commission of Finnish Power Companies, Helsinki, 321 p.

Popov, Y.A., Pevzner, S.L., Pimenov, V.P., Romushkevich, R.A., 1999. New geothermal data from the Kola superdeep well SG-3. Tectonophysics 306, 345–366.

Posiva, 2012. Olkiluoto site description 2011. Posiva Oy (Finland), Posiva Report 2012-02, 1029 p.

Pruess, K., 2006. Enhanced geothermal systems (EGS) using CO2 as working fluid—A novel approach for generating renewable energy with simultaneous sequestration of carbon. Geothermics 35, 351–367.

Purkamo, L., Bomberg, M., Kietäväinen, R., Salavirta, H., Nyyssönen, M., Nuppunen-Puputti, M., Ahonen, L., Kukkonen, I., Itävaara, M., 2016. Microbial co-occurrence patterns in deep Precambrian bedrock fracture fluids. Biogeosciences 13, 3091–3108.

Ranjram, M., Gleeson, T., Luijendijk, E., 2014. Is the permeability of crystalline rock in the shallow crust related to depth, lithology or tectonic setting? Geofluids 15, 106–119.

Rhén, I., Forsmark, T., Hartley, L., Joyce, S., Roberts, D., Gylling, B., Marsic, N., 2009. Bedrock hydrogeolology, model testing and synthesis, site descriptive modelling SDM-Site Laxemar. Swedish Nuclear Fuel and Waste Management Co. Report R-08-91 415–p. https://www.skb.com/publication/1989392/R-08-91.pdf.

Schill, E., Genter, A., Cuenot, N., Kohl, T., 2017. Hydraulic performance history at the Soultz EGS reservoirs from stimulation and long-term circulation tests. Geothermics 70, 110–124.

Schmidt, P., Steeb, H., Renner, J., 2021. Investigations into the opening of fractures during hydraulic testing using a hybrid-dimensional flow formulation. Environ. Earth Sci. 80, 497. https://doi.org/10.1007/s12665-021-09767-4.

Schmittbuhl, J., Lambotte, S., Lengliné, O., Grunberg, M., Jund, H., Vergne, J., Cornet, F., Doubre, C., Masson, F., 2021. Induced and triggered seismicity below the city of Strasbourg, France from November 2019 to January 2021. Collect C R Geosci 353, 561–584. https://doi.org/10.5802/crgeos.71.

Schulze-Makuch, D., Malik, P., 2000. The scaling of hydraulic properties in granitic rocks. In: Stober, I., Bucher, K. (Eds.), 2000, Hydrogeology of Crystalline Rocks. Kluwer, Dordrecht, pp. 127–138.

Schwarz, F.W., Zhang, H., 2003. Fundamentals of Groundwater. John Wiley & Sons, p. 583.

Seale, R., Themig, D., Athans, J., 2006. Effective Stimulation of Horizontal Wells - A New Completion Method. In: Paper presented at the SPE Technical Symposium of Saudi Arabia Section. Dhahran, Saudi Arabia. https://doi.org/10.2118/106357-MS. May 2006, SPE-106357-MS.

Sharma, P., Tsang, C.-F., Kukkonen, I.T., Niemi, A., 2015. Analysis of 6-year fluid electric conductivity logs to evaluate the hydraulic structure of the deep drill hole at Outokumpu, Finland. Int J Earth Sci. https://doi.org/10.1007/s00531-015-1268-x.

Singhal, B.B.S., Gupta, R.P., 1999. Applied Hydrogeology of Fractured Rocks. Kluwer, Dordrecht, p. 400.

Smalley, P.C., Blomqvist, R., Råheim, A., 1988. Sr isotopic evidence for discrete saline components in stratified ground waters from crystalline bedrock, Outokumpu, Finland. Geology 16, 354–357.

Smith, L., Chapman, D.S., 1983. On the thermal effects of groundwater flow. 1. Regional scale systems. J. Geophys. Res. 88, 593–608.

Smith, M.B., Shlyapobersky, J.W., 2000. Basics of hydraulic fracturing. In: Economides, M.J., Nolte, K.G. (Eds.), Reservoir Stimulation. John Wiley & Sons, Chichester, pp. 5.1–5.28.

Stanfors, R., Rhen, I., Tullborg, E.-L., Wikberg, P., 1999. Overview of geological and hydrogeological conditions of the Äspö hard rock laboratory site. Appl. Geochem. 14, 819–834.

St1, 2018. St1 web pages, https://www.st1.fi/geolampo, accessed 2018.

Stober, I., 2011. Depth- and pressure-dependent permeability in the upper continental crust: data from the Urach 3 geothermal borehole, southwest Germany. Hydrogeol J 19, 685–699.

Stober, I., Bucher, K., 2000a. Hydrogeology of Crystalline Rocks. Kluwer, Dordrecht, p. 275.

Stober, I., Bucher, K., 2000b. Hydraulic properties of the upper continental crust: data from the Urach 3 geothermal well. In: Stober, I., Bucher, K. (Eds.), Hydrogeology of Crystalline Rocks. Kluwer, Dordrecht, pp. 53–78.

Stober, I., Bucher, K., 2007. Hydraulic properties of the crystalline basement. Hydrogeol J 15, 213–224. https://doi.org/10.1007/s10040-006-0094-4.

Townend, J., Zoback, M.D., 2000. How faulting keeps the crust strong. Geology 28, 399–402.

Veikkolainen, T., Kukkonen, I.T, Tiira, T., 2017. Heat flow, seismic cutoff depth and thermal modelling of the Fennoscandian Shield. Geophys. J. Int. (2017) 211, 1414–1427. doi:10.1093/gji/ggx373.

Walker, D., Rhén, I., Gurban, I., 1997. Summary of hydrogeologic conditions at Aberg, Beberg and Ceberg. Swedish Nuclear Fuel and Waste Management Co, Technical Report TR-97-23, 226 p.

Wenneström, M., Airo, M.-L., Elminen, T., Grönholm, S., Pajunen, M., Vaarma, M. and Wasenius, P., 2006. Urban geological mapping in the Helsinki Region. Geological Survey of Finland, Archive report K 21.42/2006/6, 94 p. (in Finnish with abstract in English).

Wu, Y.-S., Pruess, K., 2000. Integral solutions for transient fluid flow through a porous medium with pressure-dependent permeability. Int. J. Rock Mech. Min. Sci. 37, 51–61.

Zang, A., Yoon, J.S., Stephansson, O., Heidbach, O., 2013. Fatigue hydraulic fracturing by cyclic reservoir treatment enhances permeability and reduces induced seismicity. Geophys. J. Int. 195 (2), 1282–1287. https://doi.org/10.1093/gji/ggt301.

Zang, A., Zimmermann, G., Hofmann, H., Stephansson, O., Min, K.-B., Kim, K.Y., 2019. How to reduce fluid-injection-induced seismicity. Rock Mech. Rock Eng. 52, 475–493. https://doi.org/10.1007/s00603-018-1467-4.

Zoback, M.D., 2007. Reservoir Geomechanics. Cambridge University Press, New York, p. 449.

Zoback, M.D., Barton, C.A., Brudy, M., Castillo, D.A., Finkbeiner, T., Grollimund, B.R., Moos, D.B., Peska, P., Ward, C.D., Wiprut, D.J., 2003. Determination of stress orientation and magnitude in deep wells. Int. J. Rock Mechan. Mining Sci. 40, 1049–1076.